AN X-RAY TIMING ANALYSIS OF NARROW-LINE AND BROAD-LINE SEYFERT 1 GALAXIES WITH *SUZAKU*

by

Angelo R. Hollett

A THESIS SUBMITTED IN PARTIAL FULFILMENT OF
THE REQUIREMENTS FOR THE DEGREE OF

BACHELOR OF SCIENCE

in

Honours Astrophysics

(Department of Astronomy and Physics, Dr. Luigi C. Gallo supervising faculty)

.....
.....
.....
.....
.....

SAINT MARY'S UNIVERSITY

April 26, 2021

Abstract

AN X-RAY TIMING ANALYSIS OF NARROW-LINE AND BROAD-LINE SEYFERT 1 GALAXIES WITH *SUZAKU*

by *Angelo R. Hollett*

submitted on April 26, 2021:

The *Suzaku* X-ray satellite has been decommissioned since 2015, leaving us with a known catalogue of observed active galactic nuclei (AGN). This work provides a timing analysis of all broad-line and narrow-line Seyfert 1 AGN observed by the XIS instrument aboard *Suzaku*, sensitive over $\sim$ 0.5 – 10 keV. Extreme variability is a ubiquitous trait among AGN, varying in brightness on characteristic timescales of hours up to weeks. The changing brightness is associated with physical components of the AGN, leading to well established relations between variability and physical parameters, such as the black hole mass (M_{BH}). We analyze the 0.5 – 10 keV structure functions for the sample, yielding a mean power law index of 1.00 $\pm$ 0.09, and a mean break of 0.22 $\pm$ 0.04 days. Furthermore, we calculate the excess variance on 60 ks, 100 ks, and 150 ks durations and reproduce the M_{BH} vs. $\sigma^2_{\rm rms}$ relation at each timescale. We also identify strong correlations between the soft excess and $\sigma^2_{\rm rms,0.5-2keV}$ at each timescale, as well as weaker correlations between τ_{char} and β.

Contents

List of Figures

Chapter 1

INTRODUCTION

1.1 ACTIVE GALACTIC NUCLEI AND THE UNIFICATION MODEL

A small but notable fraction of galaxies observed in the universe are home to supermassive black holes (SMBHs) that are actively accreting material. Typical SMBHs will range in mass (M_{BH}) from $10^6 M_\odot$ to $10^{10} M_\odot$. As material is consumed by the black hole, the active galactic nucleus (AGN) emits in extreme intensity across all wavelengths of the electromagnetic spectrum, often outshining the contribution from stars within the host galaxy. In many cases, AGN have been found to exhibit luminosities exceeding 10^{46} erg s^{-1}.

The emission is a result of a number of physical components comprising the AGN. These components are fueled primarily by the accretion disc and the corona - a cloud of hot electrons surrounder the inner accretion disc closest to the black hole. The corona acts as an isotropic radiator, propelling UV photons from the disc to X-ray energies through inverse Compton-scattering. The geometry of such a system can give rise to other components such as a jet, a dusty torus, and other sporadic gas clouds.

These components are thought to be ubiquitous in all AGN, that is to say that AGN do not differ significantly in their overall structure, rather, we observe differences in AGN primarily as a result of our viewing angle. The general structure of an AGN is shown in Fig. 1.1.

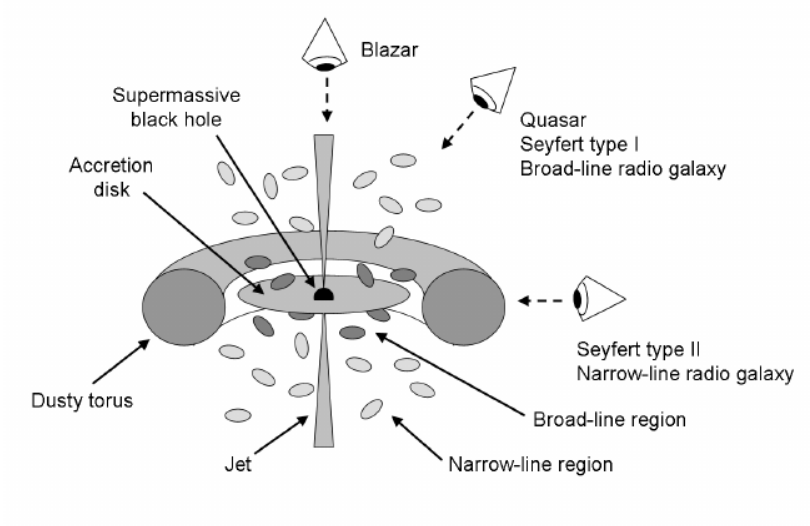

Figure 1.1: General schematic for an AGN. The viewing angle will affect certain measured properties of the AGN such as spectral lines, leading to specific classes of the AGN i.e., Seyfert type 1 and 2. A corona is implied to reside near the base of the jet. Image Credit: Zackrisson (2005).

The accretion disc of an AGN is formed when material begins its path into the black hole on a spiral track. Material in the accretion disc nearest the black hole orbits the fastest, inducing large amounts of frictional energy. This energy is radiated as a blackbody, peaking at UV wavelengths. The other components of an AGN are illuminated by this emission, therefore the SMBH and accretion disc are often referred to as the 'central engine'. This portion of the accretion disc is subject to the most intense relativistic effects. The basic structure of the central engine is depicted in Fig. 1.2.

The accretion disc can extend to upwards of several hundred gravitational radii

($r_g = GM/c^2$), with the X-ray emitting region on a scale of the order of our solar system (e.g. light hours from the black hole). The broad-line region (BLR), at larger scales, is comprised of gas and dust orbiting within the accretion disk at high velocity. Beyond the accretion disc lies the torus, formed mostly of dust and other interstellar material, extending to the scale of several parsecs. Likewise, the narrow-line region (NLR) is comprised of gas and dust as well, but extends even further to host galaxy scales. The narrow-line region remains illuminated by the central engine, emitting narrow lines due to its low velocities in the optical regime.

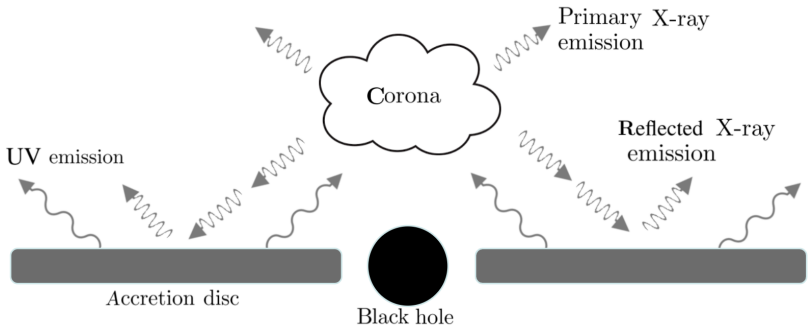

Figure 1.2: Edge-on view of the central engine of a typical AGN. The accretion disc emits UV photons through frictional processes. UV photons that encounter the corona are up-scattered to X-ray energies and emitted isotropically as the primary X-ray emission. Some X-ray photons may be reflected off the disc and produce the reflected X-ray emission. Adapted from Gallo (2011).

1.1.1 Seyfert Galaxies

There are a few main classifications of active galaxies, one of which is a Seyfert galaxy. Seyfert 2 galaxies are characterised by properties that arise from an edge-on view through the torus. The torus is sufficiently far from the SMBH so to be mostly unaffected by relativistic effects. The gas comprising the torus features lower ionisation and velocity than that of the accretion disc. Therefore, a spectrum of a characteristic Seyfert 2 will feature narrow emission lines, and some absorption

features.

A face on view of an AGN will provide a direct line-of-sight into the jet. Such AGN may be classified as quasars, or blazars in the most direct cases when jet beaming plays a major role in the apparent brightness. Active galaxies are classified as Seyfert 1 when the inclination angle takes on a more moderate value. Such angles provide a view of the innermost central region which is unobscured by the torus - as in the case of a Seyfert 2 galaxy, or the jet - as in quasars. Light originating from these regions nearest the black hole will experience relativistic effects. Emission from the BLR will be Doppler broadened. These viewing angles are depicted in Fig. 1.1.

1.1.2 Broad-line and Narrow-line Seyfert 1 AGN

Seyfert 1 galaxies are further classified into two sub-categories; broad-line Seyfert 1 (BLS1) and narrow-line Seyfert 1 (NLS1)(Osterbrock and Pogge, 1985). The distinction is based on the characteristic differences in their optical emission, in particular, the hydrogen Balmer lines. To quantify this difference, astronomers have set a cut-off based on the full-width at half-maximum (FWHM) of the observed Hβ lines. NLS1s display narrow Hβ Gaussian line profiles with a FHWM less than 2000 km s^{-1}. BLS1s show broad Gaussian line profiles with a FWHM exceeding 2000 km s^{-1} (Dewangan et al., 2001).

The discrepancies in FHWM between the two galaxy classes are a result of mechanisms driven by the physical parameters of the AGN, such as black hole mass and accretion rate. NLS1s have smaller black hole masses and higher accretion rates than

BLS1s (Nikołajuk et al., 2009; Ponti et al., 2012, see Section 1.2.1). These parameters are the foundation for the physics nearest the AGN, therefore they dictate other characteristics that arise in their spectra, separating the two classes of AGN.

A spectroscopic analysis has been performed on the same sample of AGN present in this work, and appears in Waddell and Gallo (2020) (hereafter WG20). Average spectra for each object is modelled to characterise a variety of parameters such as the photon index, luminosity, iron line profile, and soft excess, among others. WG20 confirm a previously result that NLS1s display larger photon indices than those found in BLS1s. Furthermore, WG20 find that the X-ray Eddington ratio is the primary source of variation within the sample of AGN, and that certain correlations are present in NLS1s while BLS1s do not display the same correlations. This suggests a common mechanism driving the correlations observed in NLS1s, such as a blurred reflection model, while an ionised partial covering model, or warm Comptonisation model may be a more accurate representation of the inner workings of BLS1s.

1.2 VARIABILITY IN ACTIVE GALACTIC NUCLEI

Among the many of their interesting properties, rapid variability of the brightness of AGN is one of the first characteristics to take note of. Large changes in brightness over both short and long timescales is an intrinsic property of AGN (Marshall et al., 1981; McHardy, 1989; Gallo et al., 2018). Order of magnitude changes in brightness

are often observed within hours (Gallo et al., 2004; Pinto et al., 2018). The rapid and intense variability of AGN across all wavelengths can be linked to changing components of the physical structure of AGN. Therefore, by studying AGN variability we can understand the physical components of these systems and how they evolve over time.

The X-ray emitting region of AGN resides closest to the black hole, where the accretion disc is the hottest. Like other wavelength regimes of AGN, this region is characterised by intense brightness and variability. The emitting wavelength regime is directly correlated to a characteristic timescale that the regime varies on. Therefore, the X-ray regime displays the most rapid variability, often requiring the distinction of flux states of the source. Individual variations can be characterised by hourly timescales, while flux states have been resolved over decades (Tripathi et al., 2020). Typical variations can show order of magnitude changes in brightness within hours up to years.

NLS1s typically display variability on shorter timescales than BLS1s. That is to say that NLS1s will change their brightness quicker than BLS1s, and will do so at greater amplitudes. It has been demonstrated that this property can be utilised to produce estimates for the black hole mass (Markowitz and Edelson, 2004; Papadakis, 2004b; O'Neill et al., 2005). However, the variability of accreting systems also depends on the accretion rate, thus, the black hole mass, varibility, and accretion rate, are closely linked parameters of AGN.

It has been previously suggested that AGN variability scales only with the luminosity (Barr and Mushotzky, 1986; Nandra et al., 1997; Markowitz and Edelson,

2004). However, an alternative suggestion is that the classes are dictated by mass scaling laws (Nikolajuk et al., 2004). This idea is supported by previous works that have shown NLS1 and BLS1 distributions to appear identical after applying mass corrections (Ponti et al., 2012).

1.2.1 Excess Variance

One method of quantifying the variability in AGN is to compute the excess variance in a light curve. The excess variance can be described as a measure of the amplitude of variability within a given time series (Nandra et al., 1997). There are a number of well-known correlations between AGN parameters and the excess variance, such as the black hole mass, and the power-law slope. In fact, the first application of excess variance to AGN was to probe for an anti-correlation between variability and luminosity (Nandra et al., 1997). It has been suggested that this relation is simply due to the more fundamental correlation between variability and black hole mass (Papadakis, 2004a). Such a correlation agrees with theoretical predictions that characteristic disc time scales should depend linearly on the black hole mass (Treves et al., 1988).

This project will adopt a variety of analysis techniques, and will feature applications of excess variance similar to those presented in (Ponti et al., 2012). Within the study, the group performed a timing analysis on a sample consisting of 161 AGN. The group computes the excess variance for the sample on a variety of time scales, from 10 ks up to 80 ks, and in energy bands of 0.3 – 0.7, 0.7 – 2, and 2 – 10 keV. With this, they report a strong correlation between the excess variance and the black

hole mass. Their results are in agreement with mass measurements from alternative measurement, and allow the group to estimate M_{BH} for 6 sources with no previous estimates. These results have shown that excess variance is as reliable as other techniques for estimating black hole mass, and can be applied when other techniques such as reverberation mapping (e.g. Alston et al. 2020) cannot be applied.

The group investigates other parameters that are thought to correlate with variability, such as accretion rate. The excess variance is found to correlate strongly with a number of AGN parameters. Furthermore, the correlations found within narrow-line Seyfert 1 galaxies are different from those found within samples of broad-line Seyfert 1 galaxies, but are reconciled after correcting for black hole mass (Ponti et al., 2012). This suggests that the same physical processes underlie all AGN and scale with the central black hole mass.

1.2.2 The Structure Function

The structure function is an analysis tool used to show the distribution of variability in a time series as a function of time. This technique is used with data sets that are unevenly sampled, where methods that involve Fourier transforms, like the power spectral density, (PSD; power spectrum) are more difficult to apply (Gallo et al., 2018). The structure function of AGN have a typical shape consisting of a steep positive slope at short time scales, which flattens out after a certain break time (f_b; break frequency in frequency space). This characteristic break frequency is linked to

physical properties of the AGN and scales with the central black hole mass and accretion rate (McHardy, 1989). By considering the excess variance on various timescales (i.e. 60 ks up to 150 ks) we can make a connection between regimes of the structure function that are observed in each case. Probing timescales longer than the break frequency will be linked to different variability properties than those before the break frequency.

Power spectra are often considered in variability analysis to reveal periodic behavior in black hole systems. It has been suggested that AGN are the same phenomenon as black hole X-ray binaries (BH-XRBs) scaled-up according to the black hole mass. This would be an extension of the notion that variability properties within sub-classes of AGN become identical after correcting for black hole mass (e.g. Ponti et al., 2012). González-Martín and Vaughan (2012) found further evidence that this scaling relation is true by probing PSD break frequencies for a sample of BH-XRBs. It was found that the break frequencies did in fact scale with mass, and that the scaling relations largely hold true for smaller mass black hole systems (González-Martín and Vaughan, 2012).

1.3 SUZAKU

Suzaku is a satellite telescope, designed with intent on studying X-ray photon sources (Mitsuda et al., 2007). Developed by the Japan Aerospace Exploration Agency (JAXA) in conjunction with NASA's Goddard Space Flight Center, *Suzaku* launched in 2005 with plans to operate for 2 years. *Suzaku* exceeded its plans and collected

data for 10 years before being decommissioned. Therefore, there is a complete set of AGN observed by *Suzaku*, which will be the focus of this project.

Suzaku flies in a low Earth orbit, below the inner Van Allen belts, with an orbital period of 5760 seconds, or 96 minutes. Due to this fact, observations conducted by *Suzaku* often span many orbital periods, with exposures being taken when the target source is not obscured by the Earth. Thus, *Suzaku* data analysis will often feature orbital binning, whereby the data is averaged into bins of orbital period duration.

Suzaku is equipped with four X-ray imaging Spectrometers (XIS) as well as a Hard X-ray Detector (HXD). The HXD detector utilizes a Gadolinium Silicate (GSO) scintillator in combination with silicon PIN diodes to detect photons of energies up to 600 keV (Takahashi et al., 2007). These detectors allow for excellent broad-band spectral analysis of AGN by revealing multiple energy bands that are each dominated by certain physical components of the AGN (e.g. Patrick et al. 2011, Noda et al. 2013).

This project will feature data obtained from the XIS instrument, most sensitive over 0.5 – 10 keV. This energy band features the Fe Kα complex, the coronal power law, and the soft X-ray excess as some of the most prominent features. By selecting this energy band and instrument, we will be able to better compare and contrast our results from those in previous works such as WG20 and Ponti et al. (2012).

1.4 THESIS AND PREVIOUS WORKS

This project is aimed at providing an X-ray timing analysis of a sample of AGN and will act as a compliment to the previous spectroscopic study on the same sample (Waddell and Gallo (2020), WG20, as discussed in Section 1.1.2). The data are comprised of observations of AGN conducted by the *Suzaku* satellite telescope. The individual observations in this sample are on the order of 50 ks, up to 400 ks in duration, across all detectors. The sample of sources contains AGN of varying types, including narrow-line Seyfert 1 and broad-line Seyfert 1 galaxies. The *Suzaku* instruments are capable of detecting photons from $\sim$ 0.3 to 700 keV, however, this project will focus on data collected by the XIS detector from the most sensitive region of 0.5 to 10 keV.

This work is focused on the time series for 69 individual AGN, many of which having multiple observations. The time series data between 0.5 and 10 keV have been resolved into 3 bands; 0.5 – 2.0, 2.0 – 10.0, and 0.5 – 10.0 keV by extension. In many cases the observations are separated by days, while in other cases the observations are separated by months up to years. Therefore, this work necessarily studies both short and long term variability of AGN. Furthermore, the timescales examined in this work will be considerably longer than those examined in previous studies, providing insight to variability trends on the longest timescales.

Prior to the work done by WG20, these data have not been studied systematically as a sample to examine group properties. By providing a temporal analysis within this work using the methods outlined above, we will be able to directly compare our

results to those found in WG20. (i.e. comparing spectral properties to temporal properties). These goals will help us to further determine similarities and differences between NLS1s and BLS1s. It is important that this work be completed so as to complete the temporal side of analysis which will act to comprise a comprehensive study of the data set.

Chapter 2

SAMPLE AND DATA REDUCTION

2.1 DATA SAMPLE

All *Suzaku* observations utilised in this work are publicly available on the DARTS[1] website. The sample of sources featured in this work are based on the sample utilised in WG20. This sample is derived from the 350 sources that were observed by the *Suzaku* satellite from its launch in 2006 until the end of the mission in 2015. Classification revealed 225 Seyfert galaxies in the sample. Of these sources, 106 were subclassified into Seyfert type-1 galaxies.

Seyfert 1, 1.2 and 1.5 galaxies were selected from the sample, omitting sources that display strong X-ray absorption due to an obscured view through the torus. Sources were selected that contain intrinsic (host-galaxy) column-densities of no more than 10^{22} cm^{-2}. This was done to allow the soft-excess (low energy emission) to be well constrained. A maximum redshift of $z < 0.5$ was also imposed on the sample, ensuring that all intrinsic source spectra were measured down to ~ 1 keV.

NLS1s and BLS1s are classified by the FWHM of their Hβ lines, with NLS1s exhibiting a FWHM < 2000 km s^{-1}. This resulted in the identification of 24 NLS1s

[1] `https://darts.isas.jaxa.jp/astro/suzaku/links.html`

and 49 BLS1s. ESO 323-G077 was removed from the sample of WG20 due to the source being borderline Seyfert 1/2 galaxy (Schmid, H. M. et al., 2003), and remains absent from this sample for the same reason. Mrk 1239 was removed from the sample of WG20 due to its atypical spectra (Buhariwalla et al., 2020), but remains in this work as the data are suitable for a timing analysis.

Therefore, 23 NLS1s and 47 BLS1s comprise the total sample of 70 AGN present in this work. See Waddell and Gallo (2020) tables 1 and 2 for the full list of sources and relevant AGN parameters. The observation of Mrk 1239 was conducted on May 6, 2007 under observation ID 702031010. This work uses the data collected by the XIS0 detector during the observation, with an exposure of 63128 seconds. A total of 3282 counts were measured by the detector during the observation.

2.2 DATA REDUCTION

Standard data reduction methods have been followed as described in the *Suzaku* Data Reduction Guide[2]. For more details on the reduction process see Waddell and Gallo (2020).

Light curves were produced from the processed files using the 'lcurve' software from the HEASoft 'FTOOLS' package via the latest installation (V6.28). Light curves have been generated in the energy ranges: 0.5 – 2, 2 – 10, and 0.5 – 10 keV. The light curves are binned by *Suzaku* orbital time (5760s) as well as 1000s. Light curves

[2]`https://heasarc.gsfc.nasa.gov/docs/suzaku/analysis/abc/`

binned by 1000s have been merged for sources that contain multiple observations. For example, the light curves for the 3 observations of MCG-6-30-15 are merged and presented in Fig. 2.1. This was done to ensure that the structure functions that are constructed are well sampled and will probe the longest possible time scales (See Section 3.1).

The light curves that were binned by orbital binning have also been broken into segments of lengths 60, 100, and 150 ks when possible. This was done so that the variability could be characterized on each of these timescales.

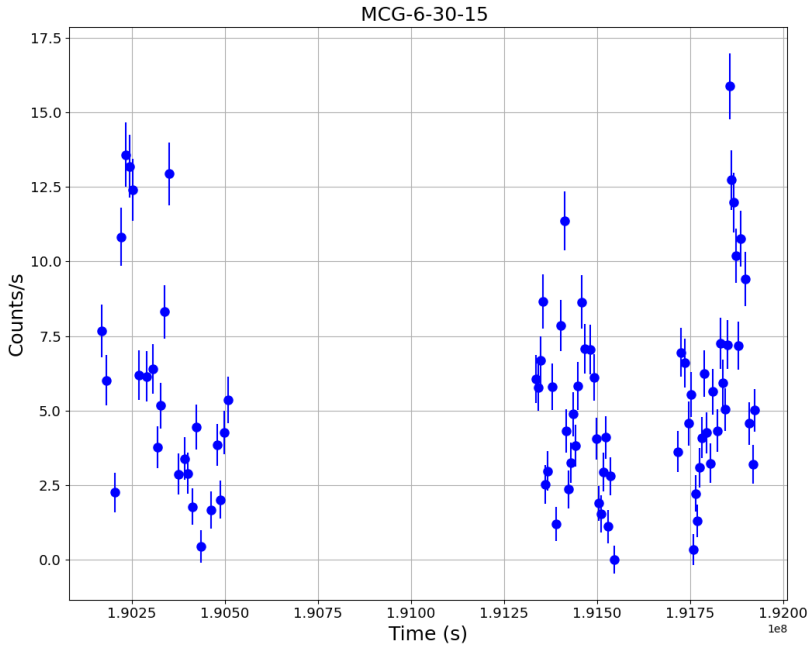

Figure 2.1: Time series for the NLS1 source MCG-06-30-15. The 0.5 – 10 keV light curve for each observation has been merged into a single light curve, retaining the relative time between each of the three observations.

Chapter 3

TIMING ANALYSIS

3.1 BUILDING A STRUCTURE FUNCTION

Structure functions have been computed using the method presented in Gallo et al. (2018). This method is available as a Python package via GitHub[1] by Derek Blue. Structure functions presented in this work have been computed over the full 0.5 – 10 keV light curves.

The benefit of using a structure function rather than a PSD is that the structure function is calculated in the time domain. This provides an appropriate method for studying the characteristic time scales of irregularly sampled light curves. Since this work features merged light curves that range in gaps spanning hours up to weeks, the structure function is highly applicable to this project. The structure function is defined by equation 3.1, from Collier and Peterson (2001):

$$SF(\tau) = \frac{1}{N(\tau)} \sum_{i<j} \left[f\left(t_i\right) - f\left(t_j\right) \right]^2 \tag{3.1}$$

Where $f\left(t_i\right)$ and $f\left(t_j\right)$ are flux measurements for a pair of points at times t_i and t_j respectively, separated by $\tau = t_i - t_j$. $N(\tau)$ is the total number of point pairs.

[1] `https://github.com/Starkiller4011/heapy`

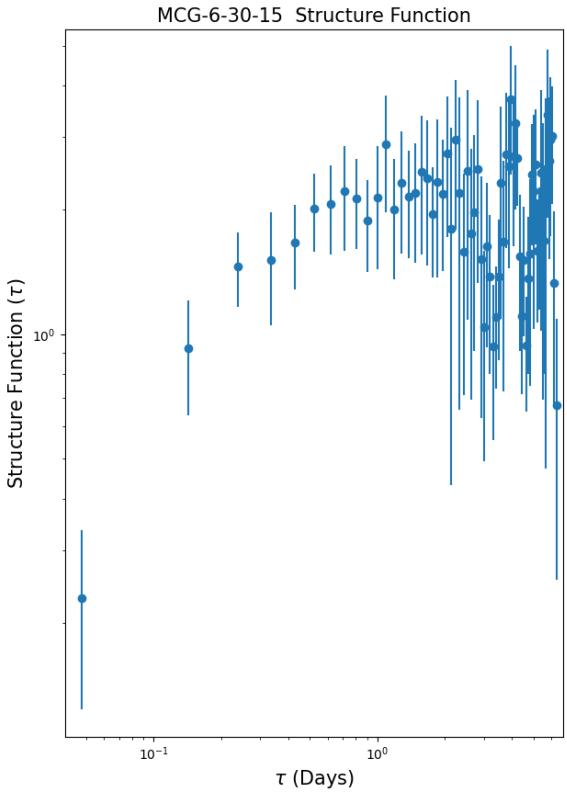

Figure 3.1: Structure function produced from the light curve of MCG-6-30-15 seen in Fig. 2.1.

The structure function is characterized by an initially steep slope which flattens beyond a certain characteristic time. The flatness degrades into noise at longer times where the data becomes unusable for analysis. An example structure function is provided in Fig. 3.1. Similar to the PSD, the initial slope is thought to be dictated by accretion parameters (Collier and Peterson, 2001; Gallo et al., 2018). The PSD slope (α) is related to the SF slope (β) by $\alpha = \beta + 1$ (Hufnagel and Bregman, 1992; Kawaguchi et al., 1998). Similarly, the characteristic break time τ_{char} is related to the PSD break frequency as $f_{char} = 1/\tau_{char}$.

The structure function was adopted in this work to test for the types of timescales that we are seeing in our sample. In doing so, it can be determined whether our

analysis inherently investigates longer or shorter time scales than those presented in previous works. That is to say that it would be inappropriate to compare correlations established in this work to previous works if the characteristic time scales being examined are substantially different.

3.2 BROKEN POWER LAW FIT TO STRUCTURE FUNCTION

Once the structure function has been computed on a given time series, it is usually the goal to determine the initial slope, as well as the characteristic break time, in order to infer the AGN properties linked to each of these parameters. This typically involves fitting a piecewise linear regression to the structure function in log space. This is tantamount to performing a bending power law fit in linear space.

A piecewise linear function is fit to the structure function in log space using the standard method of least squares minimization. The break is allowed to vary freely, along with the initial slope and intercepts. Beyond the break, the slope is fixed to a flat line. Each parameter is stepped through a pre-defined range of appropriate values which are ensured to encapsulate a realistic fit value. Errors on the slope and break time are the range of fit parameter values that are within one standard deviation of the final fit. The 'noisy' portion of the structure function is not considered during the fitting process, where the cut-off point is determined on a case-by-case basis.

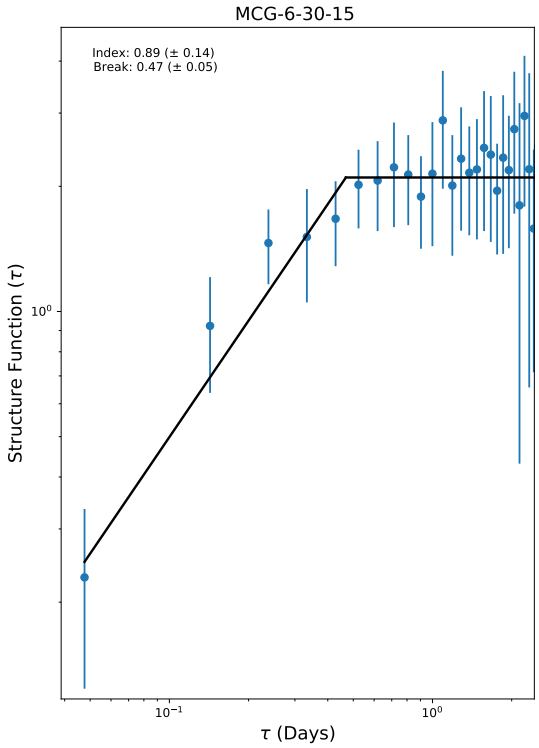

Figure 3.2: Broken power law fit to the structure function of MCG-6-30-15. The inclined portion of the power law is described by a slope, β, in log space. The slope is fixed to a flat line beyond the characteristic break time, τ_{char}.

In a number of sources, the structure functions were either of insufficient quality or were found to contain no clear break. Such sources were omitted from the broken power law fitting procedure and therefore are not included in the final measurements for β and τ_{char}. The complete set of NLS1 and BLS1 structure functions that were suitable for a broken power law fit are presented in Appendix B.

3.3 EXCESS VARIANCE CALCULATION

The excess variance (σ^2_{rms}) is calculated as per the equation in Nandra et al. (1997),

$$\sigma^2_{\rm rms} = \frac{1}{N\mu^2} \sum_{i=1}^{N} \left[(X_i - \mu)^2 - \sigma_i^2 \right] \tag{3.2}$$

for N bins in a light curve, where μ is the unweighted mean of the count rates, X_i, with errors σ_i. The uncertainty in the excess variance is calculated using equation A.1 in Appendix A.

The excess variance has been computed using Equation 3.2 for each light curve segment length; 60, 100, and 150 ks ($\sigma^2_{\rm rms,60}$, $\sigma^2_{\rm rms,100}$, $\sigma^2_{\rm rms,150}$) in each energy band (0.5 – 2 keV (soft) and 2 – 10 keV (hard)). The minimum segment length of 60 ks is chosen to retain at least 10 data points in each segment, ensuring the counting statistics remain viable. The maximum duration used is 150 ks, though there are only a few sources with available light curves spanning longer durations. The calculated excess variances for each segment length was then averaged by segment and by object.

By computing the excess variance, correlations (or lack thereof) can be established between the variability and other AGN parameters. Ponti et al. (2012) have found a number of relations between the excess variance and parameters such as accretion rate, the spectral photon index (Γ), the bolometric luminosity, and more. The results of Ponti et al. (2012), however, are restricted to shorter timescales of 10 ks up to 80 ks. This work aims at investigating the nature of such correlations at the longest timescales using the spectroscopic analysis results of WG20.

Chapter 4

RESULTS AND DISCUSSION

4.1 RESULTS

The processes described in Chapter 3 have been applied to each source in the sample, resulting in excess variance measurements for each source on 60, 100, and 150 ks light curve durations, as well as the structure function β and τ_{char} when possible.

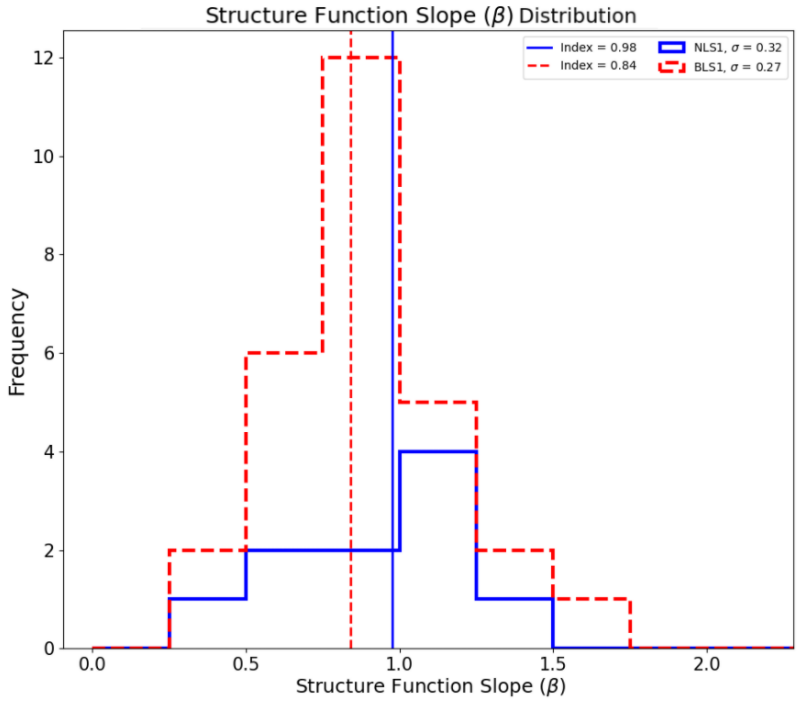

Figure 4.1: Distributions for the measured structure function slopes (β) for NLS1s and BLS1s. The NLS1 distribution is shown as a solid blue line, with the median value represented by the vertical solid blue line. The BLS1 distribution is shown as a red dashed line, with the median value appearing as a vertical red dashed line. KS test p-value = 0.27.

Distributions for the measured structure function slopes and break times are shown in Fig. 4.1 and Fig. 4.2 respectively. In each case, a Kolmogorov-Smirnov (KS) test was performed via PYTHON using SCIPY.STATS.KS_2SAMP()[1] for the NLS1 and BLS1 distributions.

The KS test returned a p-value of 0.27 and 0.01 for the slope and break distributions respectively. This indicates that, in the case of β, we cannot reject the null hypothesis that the two distributions are drawn from the same sample. Meanwhile, the p-value for the break distribution suggests that the null hypothesis may be rejected, that is to say that the two distributions are drawn from different samples.

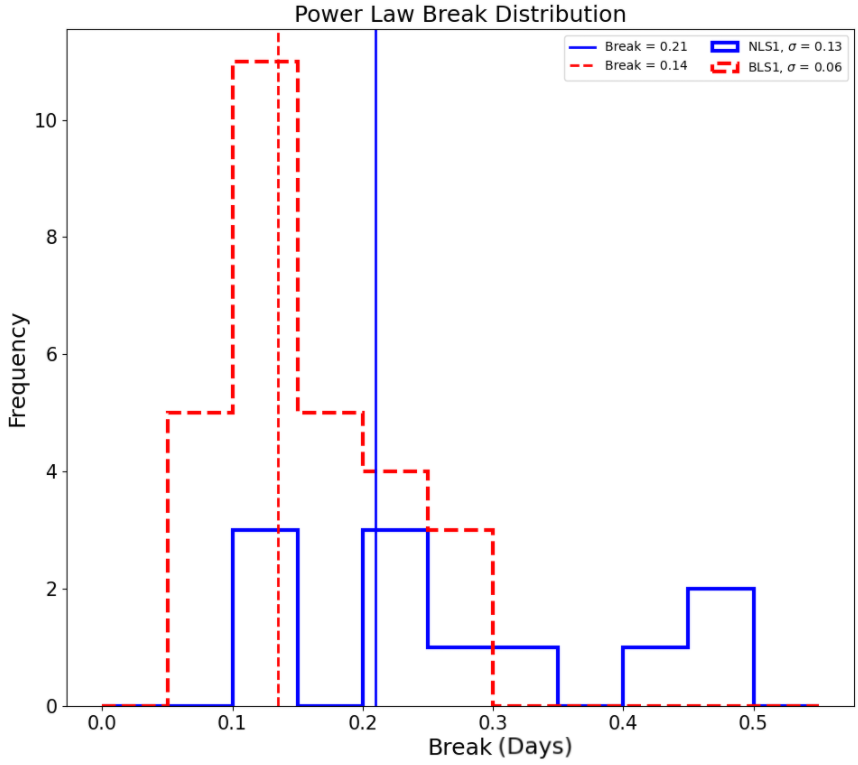

Figure 4.2: Distributions for the measured structure function break time (days) (τ_{char}) for NLS1s and BLS1s. The NLS1 distribution is shown as a solid blue line, with the median value represented by the vertical solid blue line. The BLS1 distribution is shown as a red dashed line, with the median value appearing as a vertical red dashed line. KS test p-value = 0.01.

[1] `https://docs.scipy.org/doc/scipy/reference/generated/scipy.stats.ks_2samp.html`

The excess variance calculations performed on this sample have confirmed a known property that AGN vary similarly in each energy band on short time scales (e.g. Ponti et al. 2012), but slightly favor more variability in the soft band (e.g. Chitnis et al. 2009). This can be shown by plotting the excess variance in two bands against each other (See Fig. 4.3).

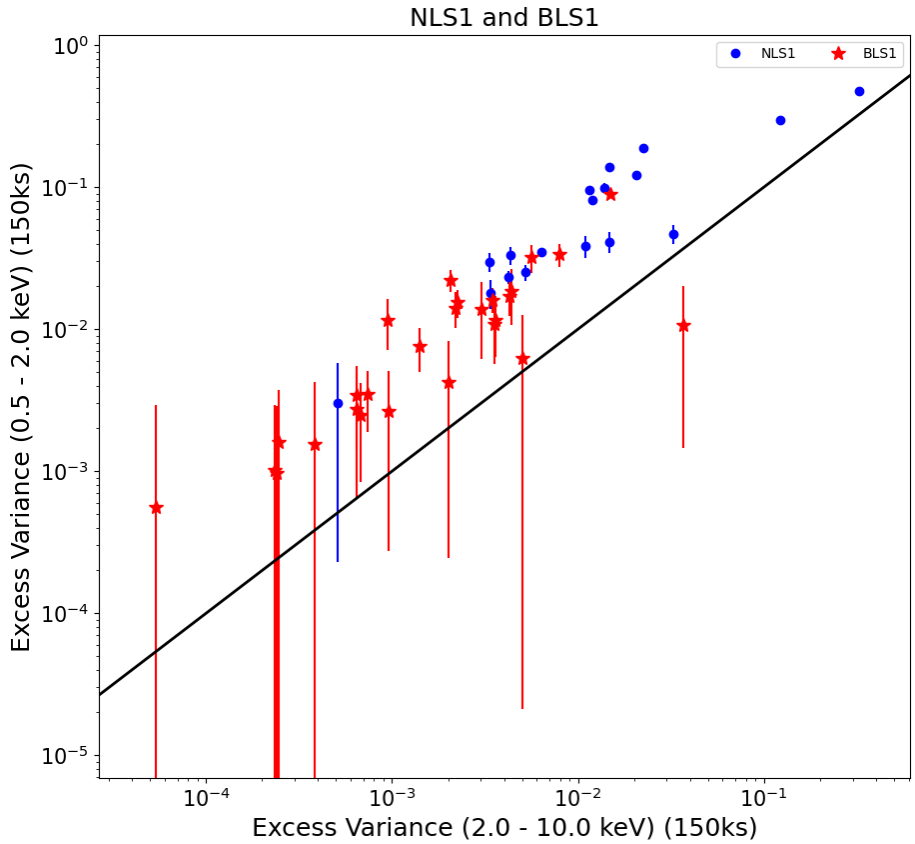

Figure 4.3: Excess variance in the hard (2-10 keV) band vs. excess variance in the soft (0.5 – 2 keV) band calculated in 150 ks durations. The solid black line is the one to one line expected when the variability is equivalent in both bands.

4.2 CORRELATIONS WITH AGN PARAMETERS

A correlation search was performed using the results of this work (β, τ_{char}, $\sigma^2_{\mathrm{rms,60,0.5-2keV}}$, $\sigma^2_{\mathrm{rms,60,2-10keV}}$, $\sigma^2_{\mathrm{rms,100,0.5-2keV}}$, $\sigma^2_{\mathrm{rms,100,2-10keV}}$, $\sigma^2_{\mathrm{rms,150,0.5-2keV}}$, $\sigma^2_{\mathrm{rms,150,2-10keV}}$) along with several of the spectral paremeters of WG20 (M_{BH}, Γ, Soft excess (SE), Hard excess (HE)). In each case, the Pearson correlation coefficient (r) was computed for a linear regression produced via least squares minimization. The correlation search and fitting procedure was performed separately on the NLS1 and BLS1 samples.

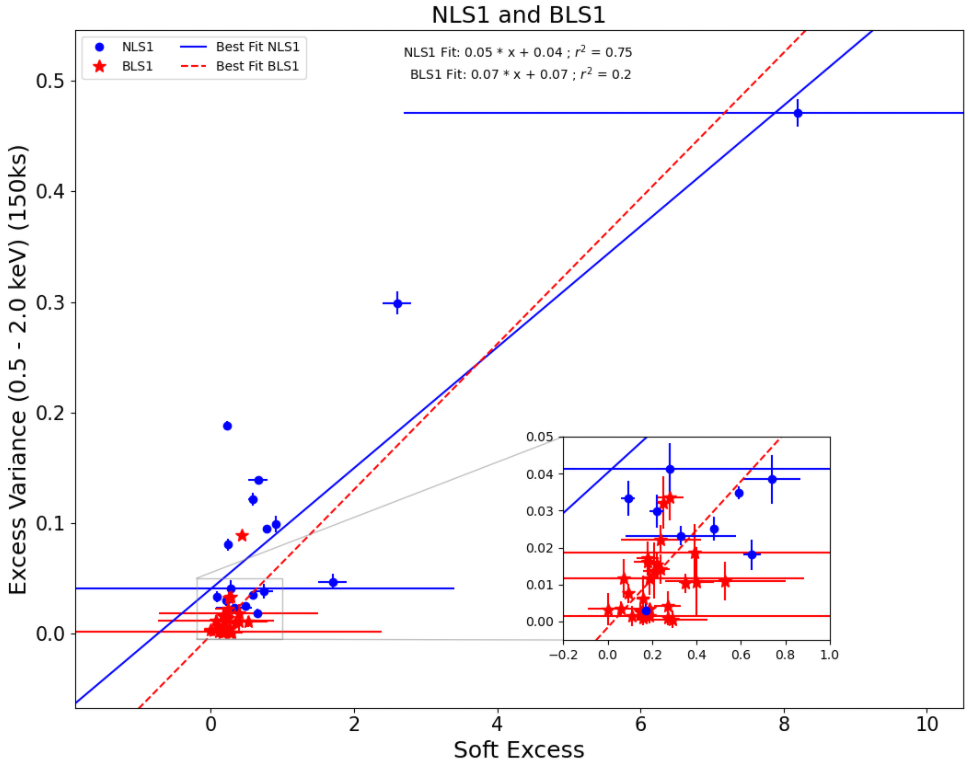

Figure 4.4: Correlations established between the excess variance in the soft band on the 150 ks timescale ($\sigma^2_{\mathrm{rms,150,0.5-2keV}}$) and the soft excess (SE) for NLS1s and BLS1s. The NLS1 best fit line is shown as a solid blue line. The BLS1 best fit line is shown as a red dashed line.

Several notable correlations were established during the search. One is found between the soft excess and $\sigma^2_{\mathrm{rms,150,0.5-2keV}}$. The r value was found to be ~ 0.87 ($r^2 = 0.75$) for the NLS1s, indicating a strong correlation. This result is potentially anticipated, and is discussed further in Section 4.3. The BLS1s display a weaker correlation, and are clustered at smaller values of each parameter. The correlation is presented in Fig. 4.4.

A weaker, but still notable correlation was also established between structure function slope (β) and the break time (τ_{char}). The anti-correlation in both the NLS1 and BLS1 samples are shown in Fig. 4.5. Although r was found to be lower than some of the other correlations, it is important to notice the distributions of the two groups with respect to each other. The BLS1s are clustered around smaller values of both the break and slope, while the NLS1s adopt a larger spread, with fewer points appearing at small values.

This work also allows us to check for a correlation between excess variance and the black hole mass. The correlation between AGN variability in the X-ray band and black hole mass has been established and reproduced many times (e.g. Lu and Yu 2001; Papadakis 2004b; O'Neill et al. 2005; Zhou et al. 2010; Ponti et al. 2012). The results of the excess variance calculations allow us to consider this relation on longer timescales (60 ks up to 150 ks). This is useful in comparison to the work of Ponti et al. (2012) who establish the relation on 10 ks up to 80 ks. We find a strong relation between the excess variance and M_{BH} on each timescale. Fig. 4.6 shows the relation between $\sigma^2_{\mathrm{rms,150,0.5-2keV}}$ and M_{BH}.

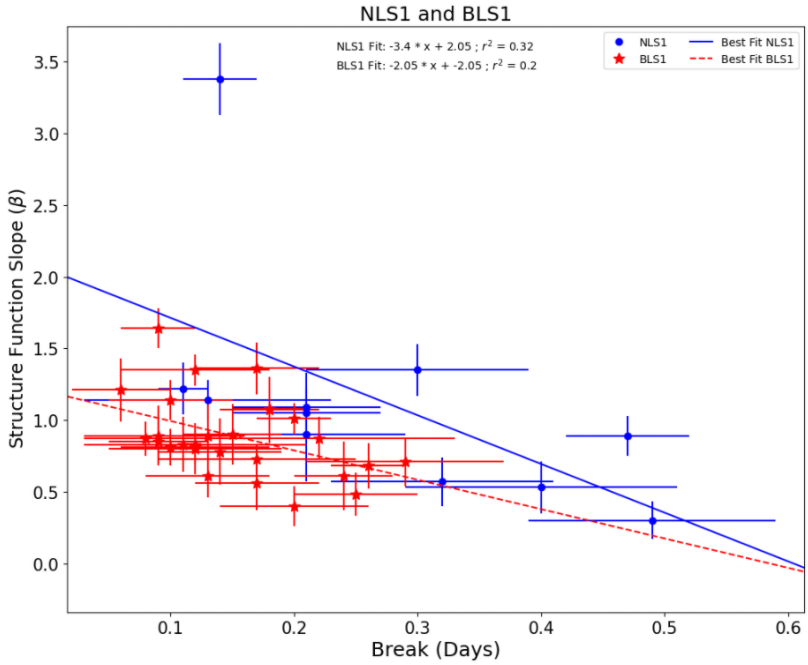

Figure 4.5: Correlations established between the structure function slope (*beta*) and the break time in days, (τ_{char}) for NLS1s and BLS1s. The NLS1 best fit line is shown as a solid blue line. The BLS1 best fit line is shown as a red dashed line.

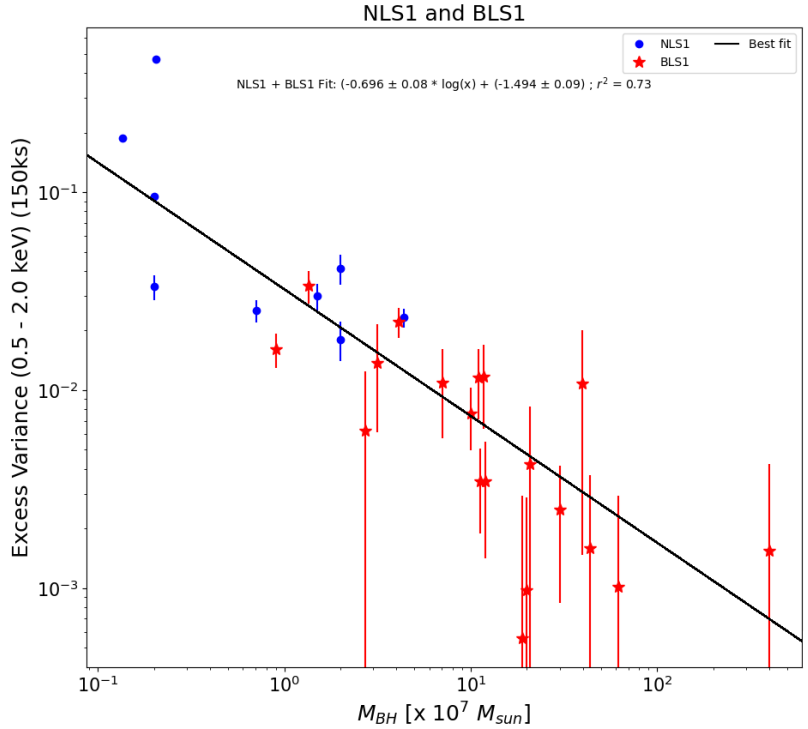

Figure 4.6: $\sigma^2_{\mathrm{rms},150,0.5-2\mathrm{keV}}$ vs. M_{BH} relation for the full NLS1 + BLS1 sample. The solid black line is the best fit.

4.3 DISCUSSION

The results of our timing analysis are widely in agreement with previous works. The full sample (NLS1 + BLS1) is found to have an average β of ~ 0.91, corresponding to $\alpha = \beta + 1 = 1.91$, while our NLS1 sources yield an average of $\alpha \sim 1.97$. González-Martín and Vaughan (2012) find an average α of 2.0 in NLS1 sources within their sample of 104 AGN (Mix of Seyfert 1, Seyfert 2, and BLLAC AGN). We find an average break time of ~ 0.22 days while González-Martín and Vaughan (2012) find an average of ~ 0.034 days, although the bending power law is not the favored model in their sample. This indicates that the timescales of variability observed in our sample are quite long. Our timescales, however, are still within reasonable values found in previous works (e.g. Uttley et al. 2002; Papadakis 2004b).

We confirm and reproduce the well known relation between M_{BH} and σ^2_{rms}. This relation is found adopting the excess variance on 60, 100, and 150 ks timescales, demonstrating that this relation is true on the longest timescales whilst confirming the previously known result on intermediate timescales. Reproducing such results provides further confidence that the results of our analysis are accurate and realistic. Furthermore, our relationship can provide estimates for M_{BH} when using data collected on similar orbital periods, e.g. *NuSTAR*.

Our correlation search has revealed several strong relationships between the results of the timing analysis in this work and the spectroscopic results of WG20. The correlation between the soft excess and $\sigma^2_{\mathrm{rms,150,0.5-2keV}}$ (Fig. 4.4) was quite strong amongst NLS1s, with an r value of ~ 0.87.

Several physical mechanisms have been proposed to explain the excess emission observed below ~ 1 keV in AGN, including Comptonized emission, reflection, or absorption (Gierliński and Done, 2004; Sobolewska and Done, 2007). Partial covering of the accretion disc by a partially ionised absorbing medium is often sufficient for describing the spectra of sources displaying a soft excess (Tanaka et al., 2004; Tripathi et al., 2019; Boller et al., 2021). Such a component will dominate the variability on short timescales (Kaastra and Barr, 1989; Boller et al., 2021). Alternative explanations for the soft excess associated with the corona (e.g. 'warm corona', Petrucci et al. 2020) will vary on longer timescales (Gallo et al., 2007; Wilkins and Gallo, 2015).

The interplay of the soft excess with variability timescales may lead us to anticipate a relationship between the soft excess and $\sigma^2_{\rm rms,0.5-2keV}$. This relation was found to be only slightly stronger in the 150 ks timescale, but was almost equally strong in 60 ks and 100 ks ($r = 0.85$ and 0.86 respectively). This may support notions that the physical components underlying the soft excess appear in all AGN and act at their respective timescales. The NLS1 1H 0707-495 is consistently found to have the largest $\sigma^2_{\rm rms,0.5-2keV}$ at each timescale, which is also known for both its extreme soft excess and intense variability (Fabian et al., 2004; Wilkins et al., 2014; Boller et al., 2021).

Although no significant correlation was found between τ_{char} and Γ, it is useful to note the distribution of the BLS1s and NLS1s within the parameter space (Fig. 4.7). The NLS1 group tends to scatter towards the top-right quadrant of the plot, while the BLS1s occupy the lower-left quadrant. This is to say that NLS1s occupy larger values of τ_{char} and Γ, while BLS1s reside at the smaller values for each parameter.

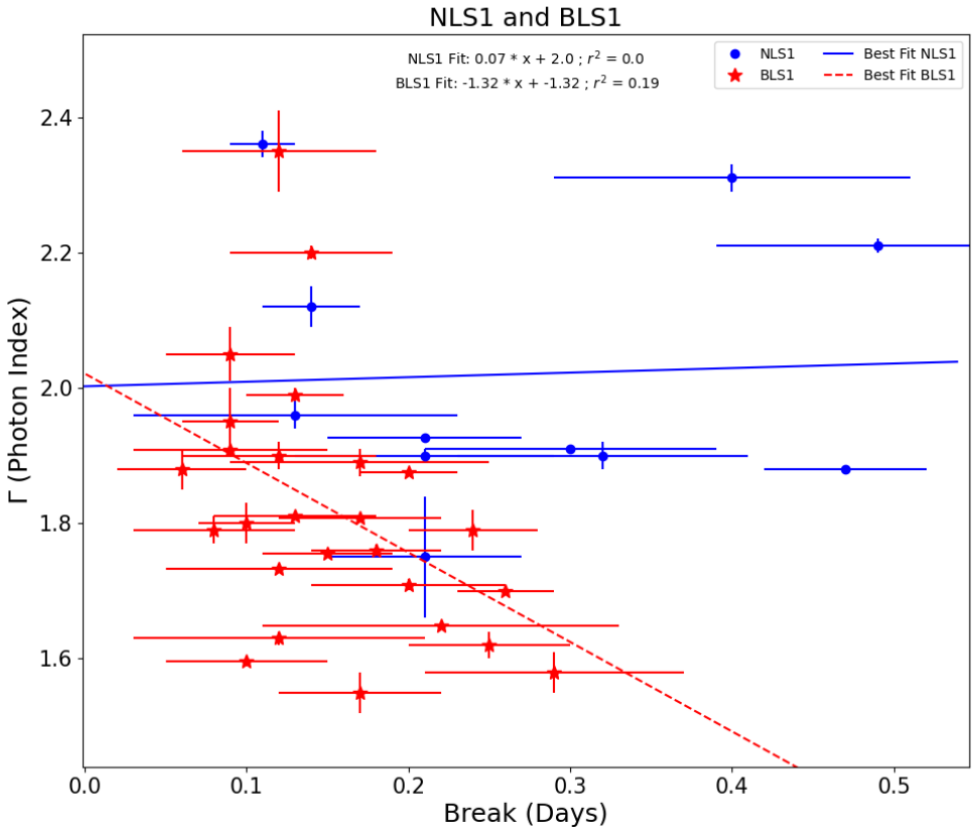

Figure 4.7: Structure function break (τ_{char}) vs. spectral photon index (Γ) for BLS1s and NLS1s. The NLS1 best fit line is shown as a solid blue line. The BLS1 best fit line is shown as a red dashed line.

Chapter 5

CONCLUSION

Presented is a timing analysis of all NLS1 and BLS1 AGN observed by the *Suzaku* satellite during its 10 year operation period. This work acts as a compliment to the spectroscopic analysis completed on the same sample by Waddell and Gallo (2020) (WG20). The sample includes many well studied sources, allowing us to directly compare our results to additional previous works.

Light curves have been constructed from data collected by the XIS instrument, following standard *Suzaku* processing techniques. Light curves have been produced in the 0.5 – 2, 2 – 10, and 0.5 – 10 keV bands, and binned by both orbital (5760s) and 1000s bins. In doing so, we have calculated the excess variance ($\sigma^2_{\rm rms}$) in each band on 60, 100, and 150 ks durations, and have analyzed the structure functions for the full 0.5 – 10 keV band.

By fitting the structure function with a broken power law we are able to measure the slope (β) and break time (τ_{char}). We find that the slopes are in agreement with previous works, with a mean value of $\alpha = \beta + 1 = 2.00 \pm 0.09$. The measurements for τ_{char} favor slightly larger values (mean $\tau_{char} = 0.22 \pm 0.04$), but are still well within the range of reasonable values. This is an indication that the sample exhibits characteristic variability on slightly longer timescales. We find a weak anti correlation between τ_{char} and β in both the NLS1s and BLS1s ($r = 0.56$ and 0.45 respectively), with the

more interesting result that NLS1s exhibiting larger values of both parameters.

Our measurements for $\sigma^2_{\rm rms,0.5-2keV}$ and $\sigma^2_{\rm rms,2-10keV}$ nearly exhibit a one to one relation, displaying slightly more variability in the soft band, in agreement with previous works. We also test for correlations with our $\sigma^2_{\rm rms}$ against literature values for black hole masses M_{BH} and reproduce the well known relation between the parameters on each time scale (60 ks, 100 ks, 150 ks). Therefore we confirm that the relation holds at even the longest timescales.

A correlation search has been performed between the parameters measured in this work along and the parameters measured in WG20. We find a strong correlation (r = 0.86) between the soft excess and $\sigma^2_{\rm rms,0.5-2keV}$ within the NLS1 sources. The correlation is roughly the same strength on each duration.

Although we do not find a strong correlation between τ_{char} and Γ in either the NLS1s or BLS1s, it is interesting to note the spread in each group. The NLS1s occupy larger values of each parameter, while the BLS1s reside at smaller values.

The NLS1 and BLS1 galaxies comprising the sample are overall typical in their characteristics with respect to other similar samples. Therefore the sample is useful in distinguishing the X-ray properties between the two groups. It would be useful to examine the sample on timescales longer than 200 ks, to test if the relations established in this work hold at even longer timescales. Only a few members of this sample have observations of such duration, therefore missions such as *eROSITA* or the future *ATHENA* satellite may prove useful in their ability to conduct long and uninterrupted observations.

Appendix A

Uncertainty in the Excess Variance

The error on the excess variance (σ^2_{rms}) is given by equation 11 in Vaughan et al. (2003):

$$\left(\Delta\sigma^2_{\rm rms}\right)_{meas} = \sqrt{\left(\sqrt{\frac{2}{N}}\frac{<\sigma_i^2>}{\mu^2}\right)^2 + \left(\sqrt{\frac{<\sigma_i^2>}{N}}\frac{2F_{\rm var}}{\mu}\right)^2} \tag{A.1}$$

Where F_{var} is the fractional variability:

$$F_{\rm var} = \sqrt{\frac{S^2 - \overline{\sigma^2_{\rm err}}}{\mu^2}} \tag{A.2}$$

and $<\sigma_i^2>$ is the mean of the squared errors, from equation 10 in Vaughan et al. (2003). S^2 is the variance:

$$S^2 = \frac{1}{N-1}\sum\left(\chi_i - \bar{\chi}\right)^2 \tag{A.3}$$

where $\bar{\chi}$ is the mean count rate.

Appendix B

STRUCTURE FUNCTIONS

B.1 Narrow Line Seyfert 1 Structure Functions

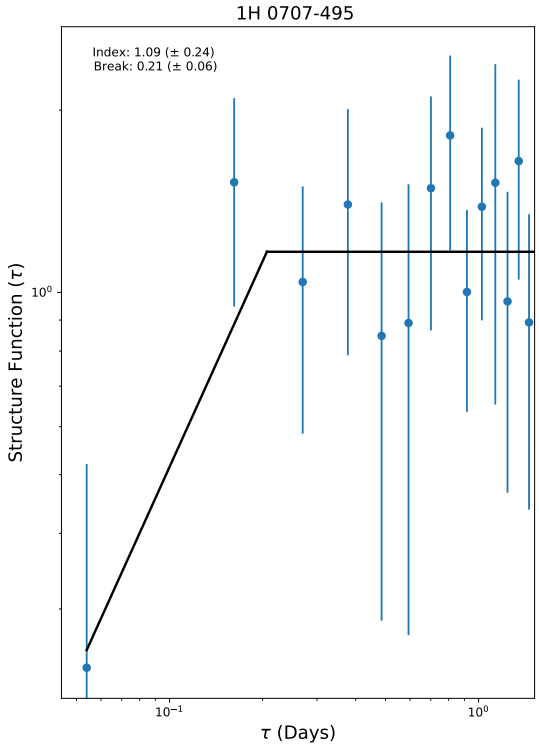

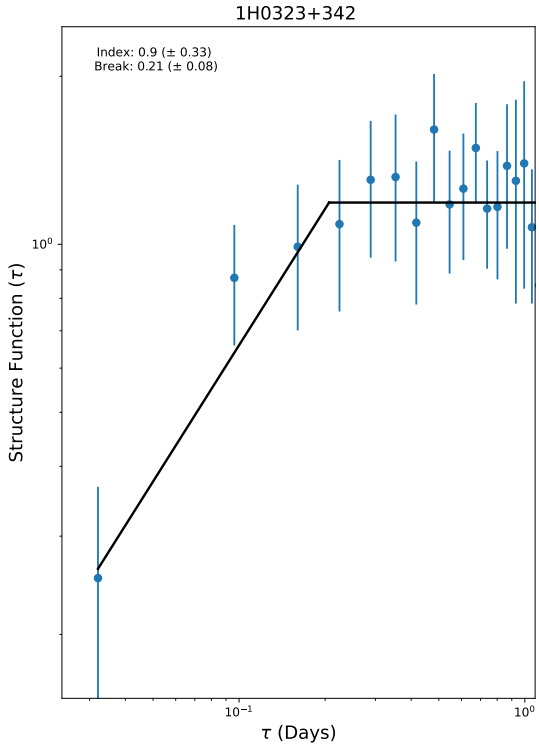

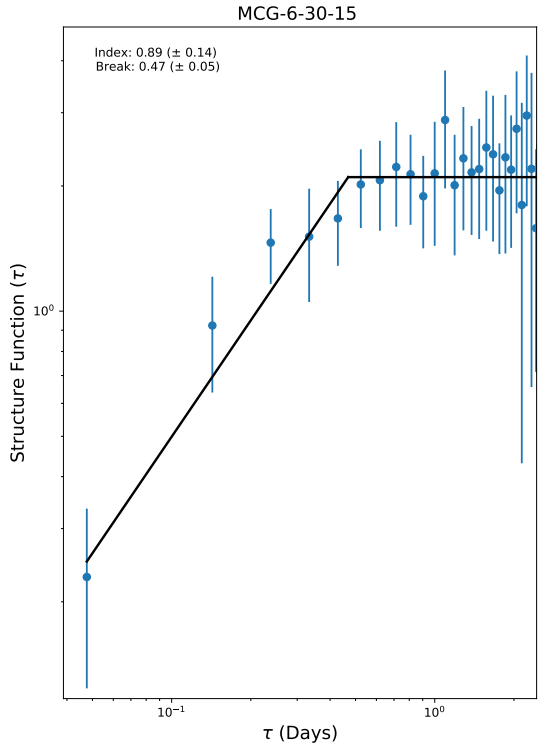
MCG-6-30-15
Index: 0.89 (± 0.14)
Break: 0.47 (± 0.05)
Structure Function (τ)
τ (Days)

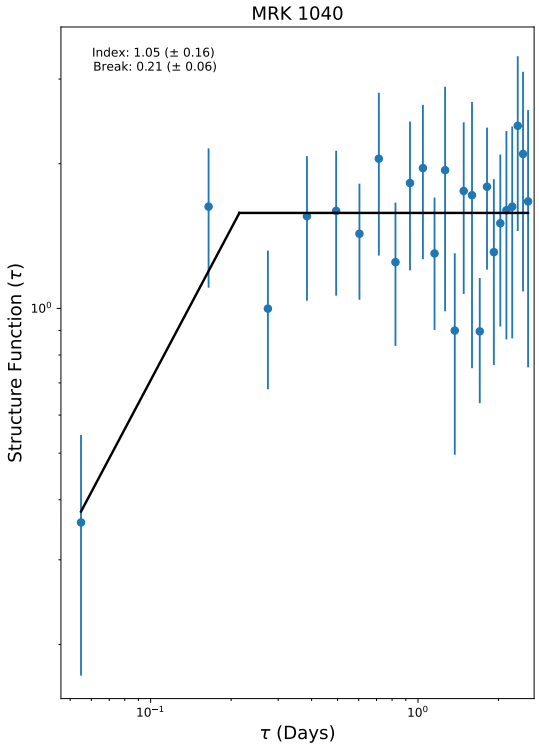
MRK 1040
Index: 1.05 (± 0.16)
Break: 0.21 (± 0.06)
Structure Function (τ)
τ (Days)

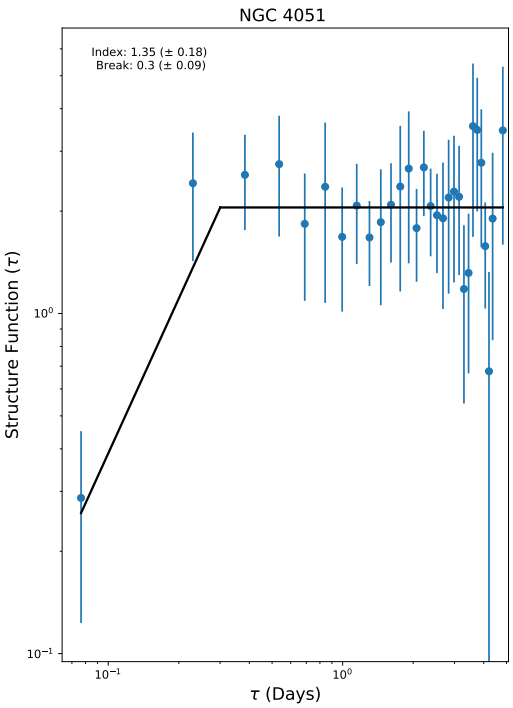
NGC 4051
Index: 1.35 (± 0.18)
Break: 0.3 (± 0.09)
Structure Function (τ)
τ (Days)

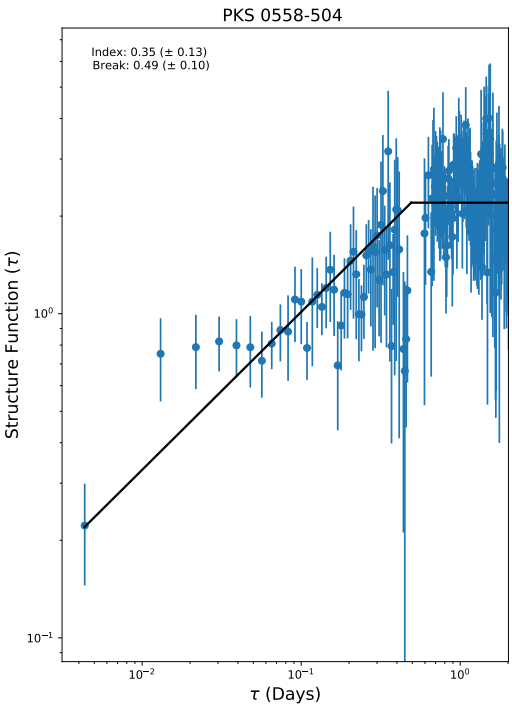
PKS 0558-504
Index: 0.35 (± 0.13)
Break: 0.49 (± 0.10)
Structure Function (τ)
τ (Days)

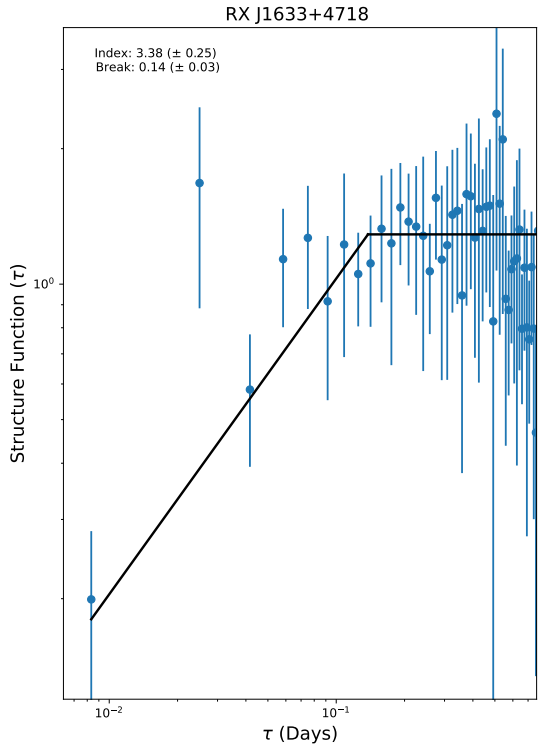
RX J1633+4718
Index: 3.38 (± 0.25)
Break: 0.14 (± 0.03)
Structure Function (τ)
τ (Days)

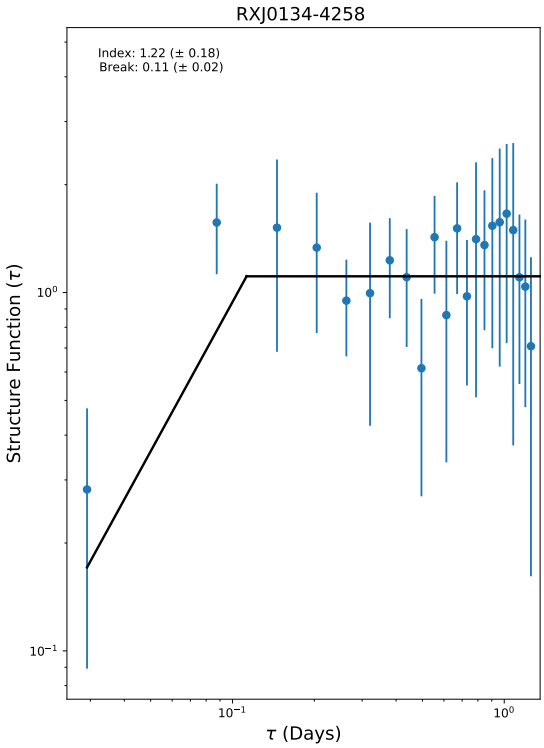
RXJ0134-4258
Index: 1.22 (± 0.18)
Break: 0.11 (± 0.02)
Structure Function (τ)
τ (Days)

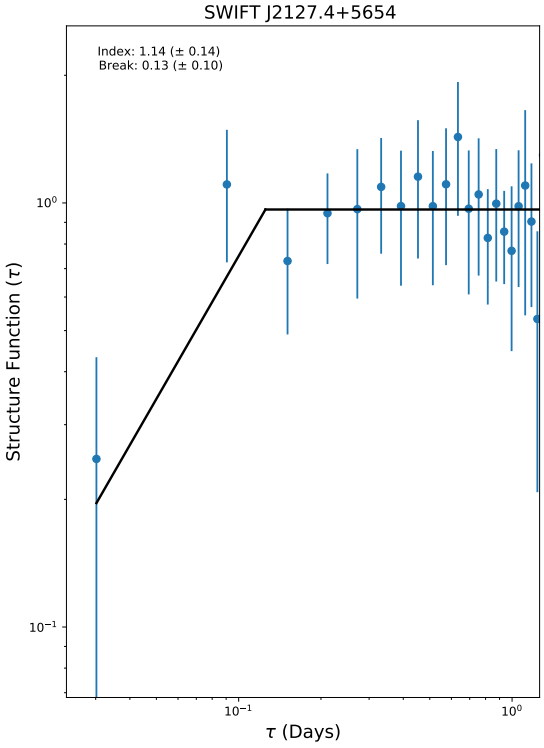
SWIFT J2127.4+5654
Index: 1.14 (± 0.14)
Break: 0.13 (± 0.10)
Structure Function (τ)
τ (Days)

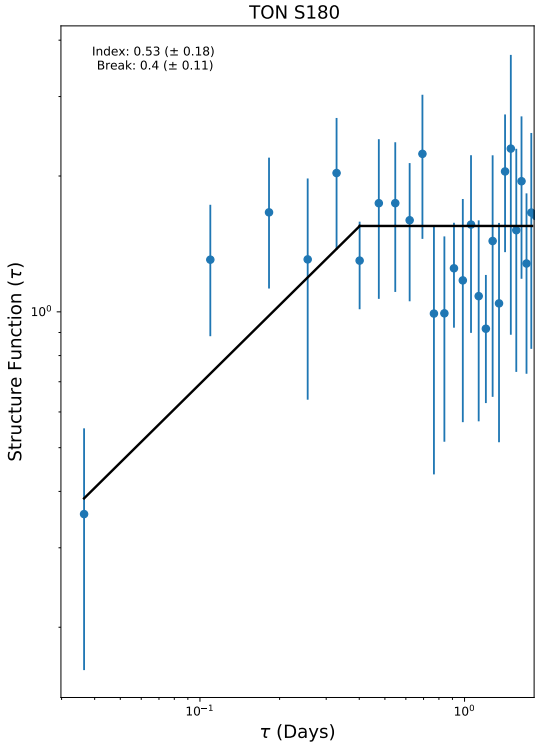
TON S180
Index: 0.53 (± 0.18)
Break: 0.4 (± 0.11)
Structure Function (τ)
τ (Days)

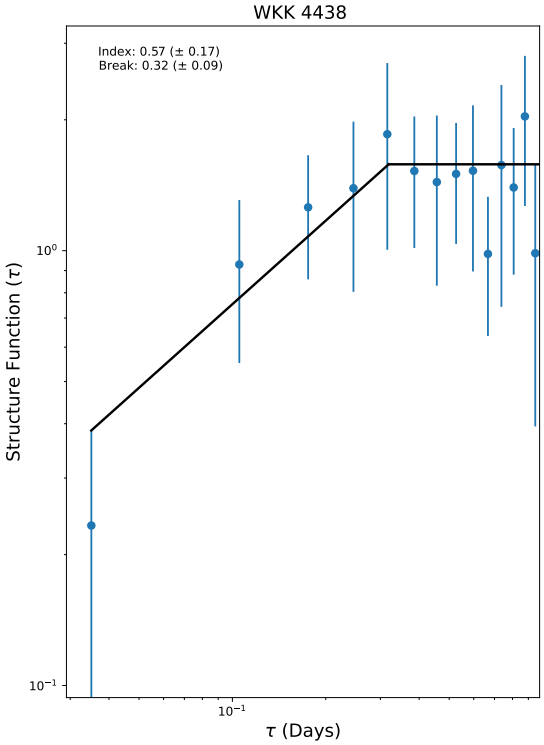
WKK 4438
Index: 0.57 (± 0.17)
Break: 0.32 (± 0.09)
Structure Function (τ)
10^{0}
10^{-1}
10^{-1}
τ (Days)

B.2 Broad Line Seyfert 1 Structure Functions

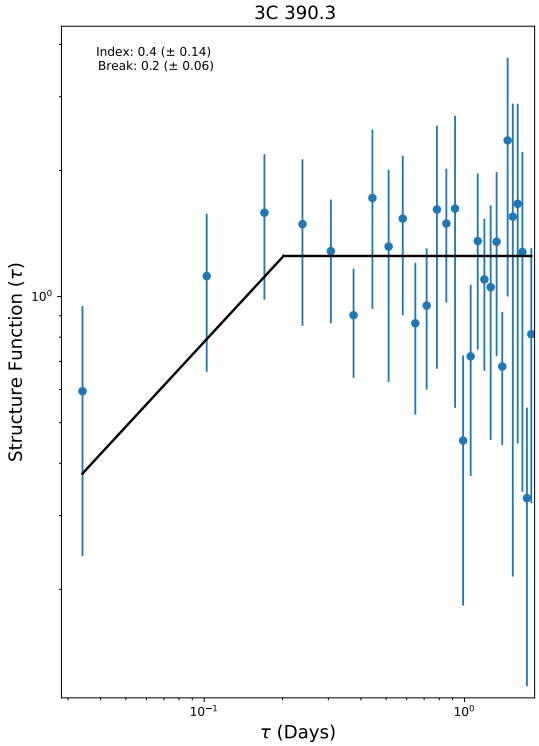

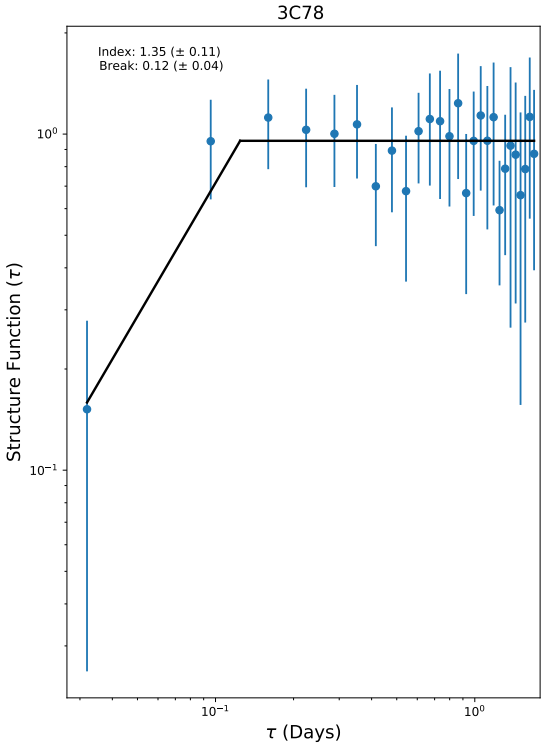

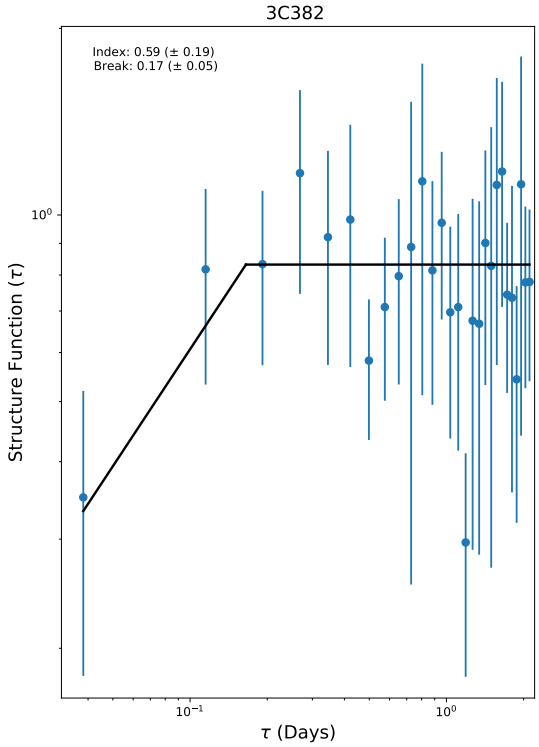

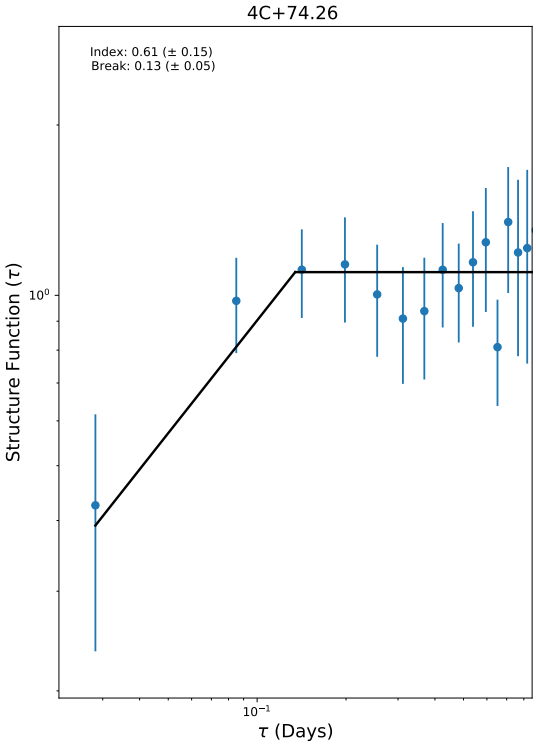

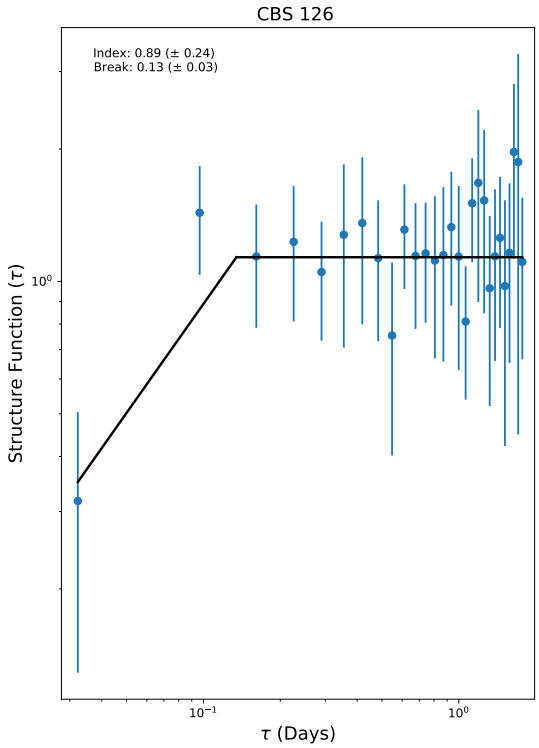
CBS 126
Index: 0.89 (± 0.24)
Break: 0.13 (± 0.03)
Structure Function (τ)
τ (Days)

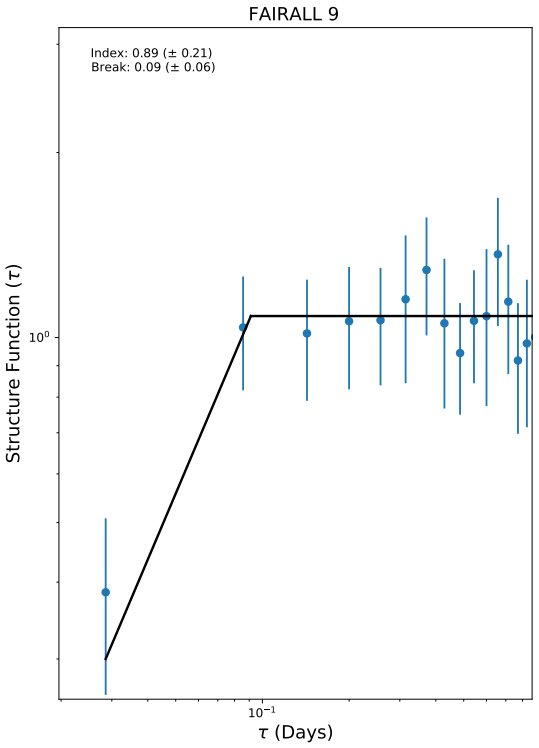
FAIRALL 9
Index: 0.89 (± 0.21)
Break: 0.09 (± 0.06)
Structure Function (τ)
τ (Days)

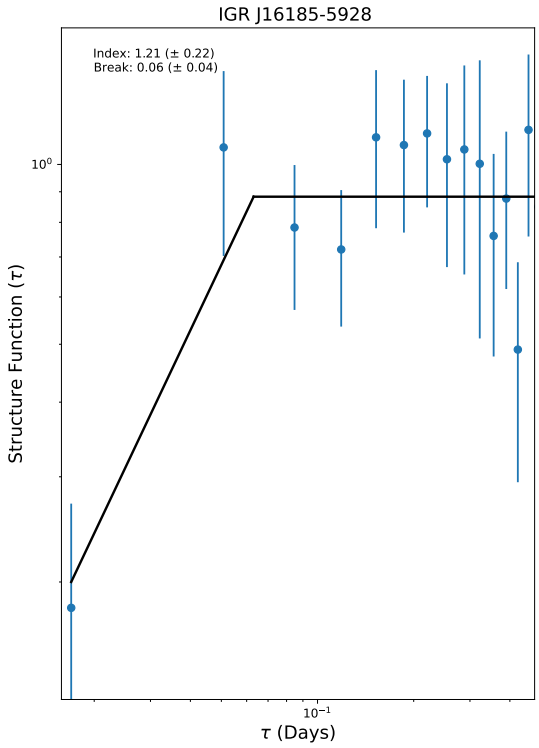
IGR J16185-5928
Index: 1.21 (± 0.22)
Break: 0.06 (± 0.04)
Structure Function (τ)
τ (Days)

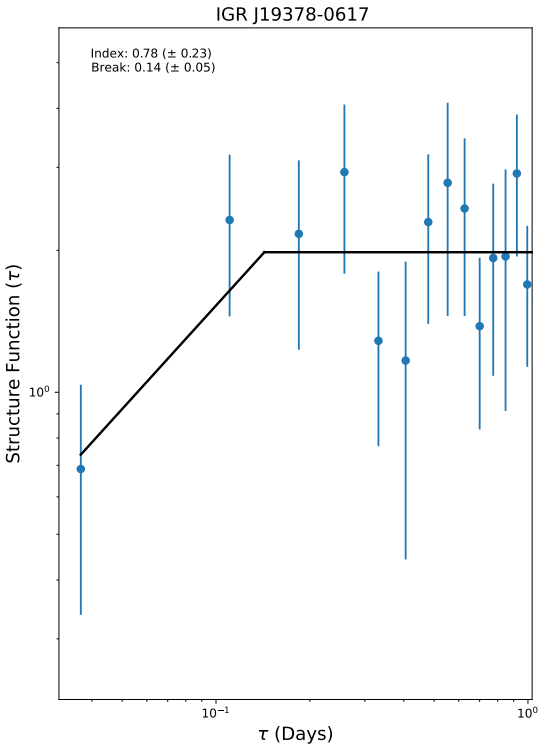
IGR J19378-0617
Index: 0.78 (± 0.23)
Break: 0.14 (± 0.05)
Structure Function (τ)
τ (Days)

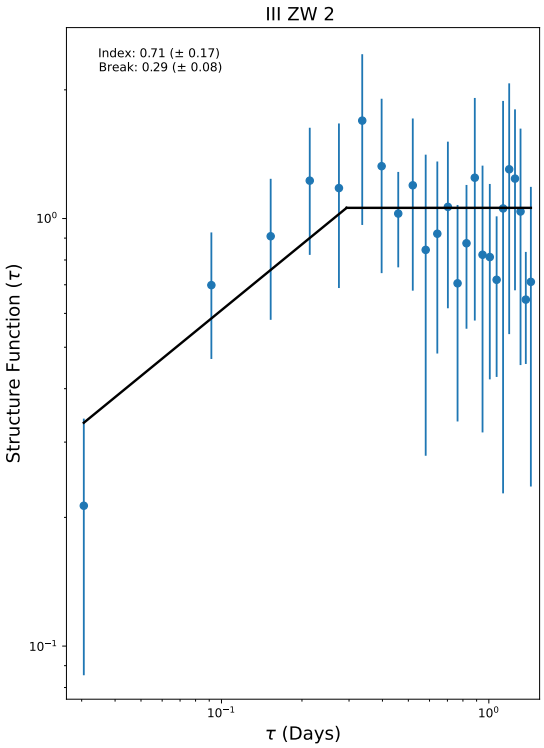
III ZW 2
Index: 0.71 (± 0.17)
Break: 0.29 (± 0.08)
Structure Function (τ)
τ (Days)

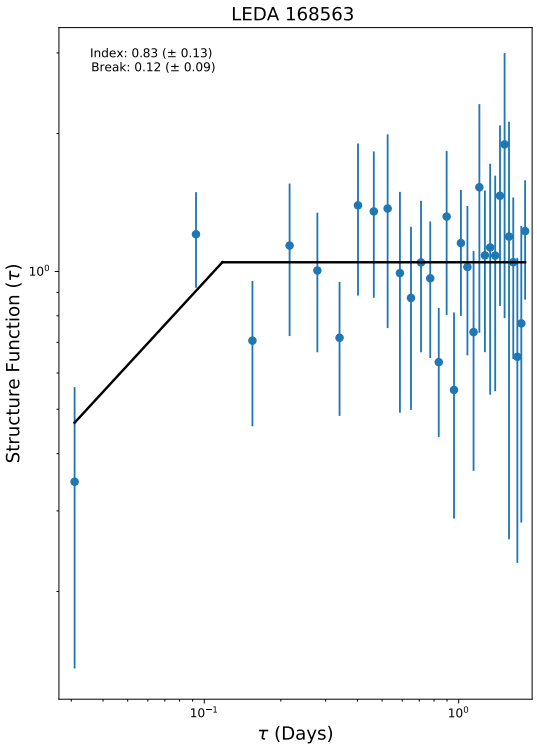
LEDA 168563
Index: 0.83 (± 0.13)
Break: 0.12 (± 0.09)
Structure Function (τ)
τ (Days)

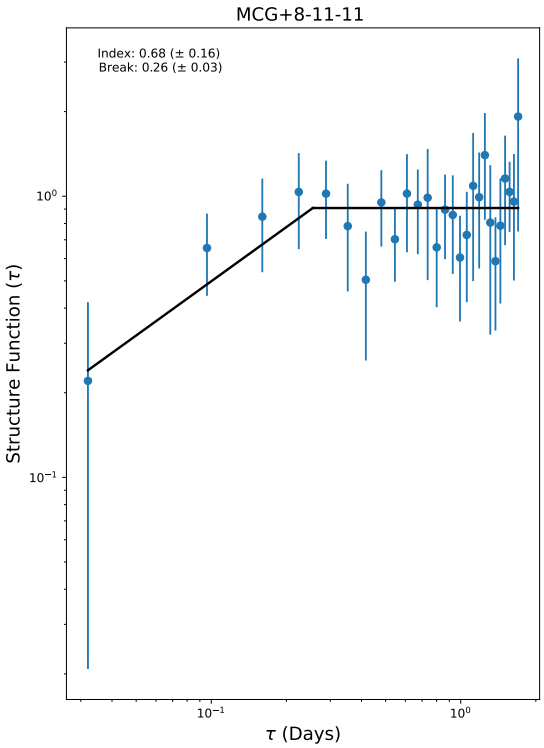
MCG+8-11-11
Index: 0.68 (± 0.16)
Break: 0.26 (± 0.03)
Structure Function (τ)
τ (Days)

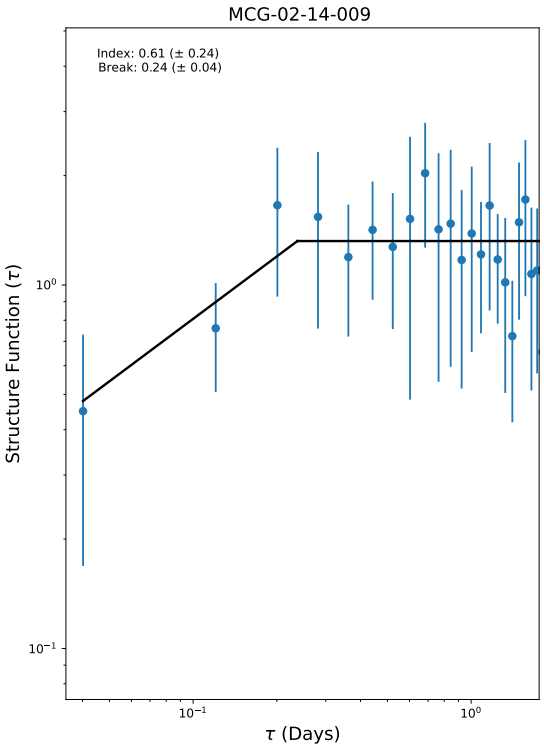
MCG-02-14-009
Index: 0.61 (± 0.24)
Break: 0.24 (± 0.04)
Structure Function (τ)
τ (Days)

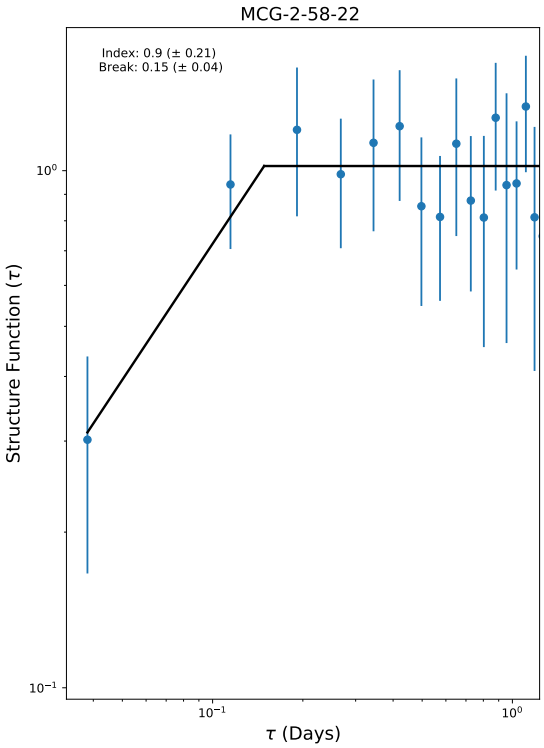
MCG-2-58-22
Index: 0.9 (± 0.21)
Break: 0.15 (± 0.04)
Structure Function (τ)
τ (Days)

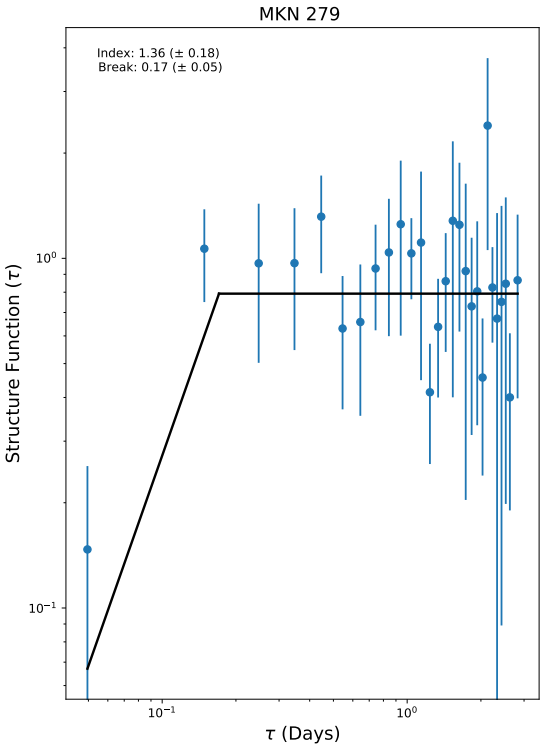
MKN 279
Index: 1.36 (± 0.18)
Break: 0.17 (± 0.05)
Structure Function (τ)
τ (Days)

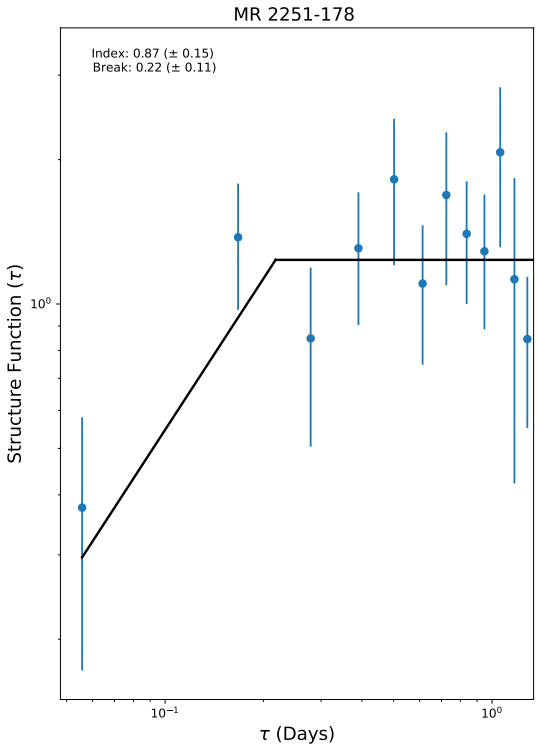
MR 2251-178
Index: 0.87 (± 0.15)
Break: 0.22 (± 0.11)
Structure Function (τ)
τ (Days)

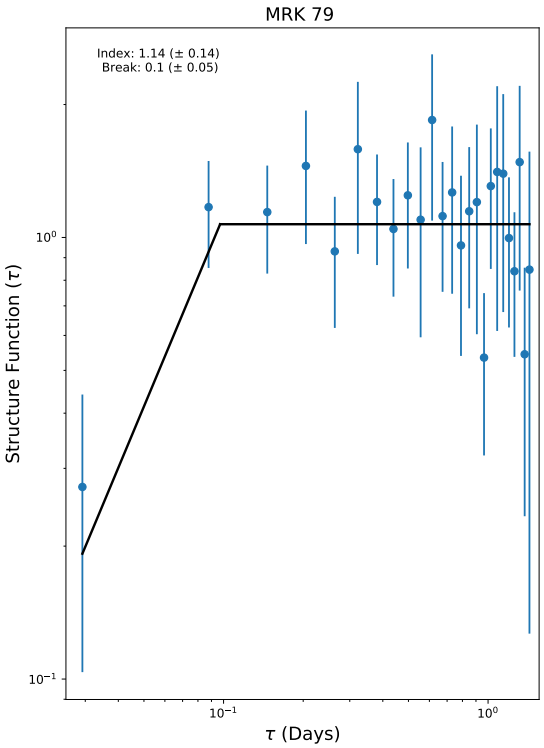
MRK 79
Index: 1.14 (± 0.14)
Break: 0.1 (± 0.05)
Structure Function (τ)
τ (Days)

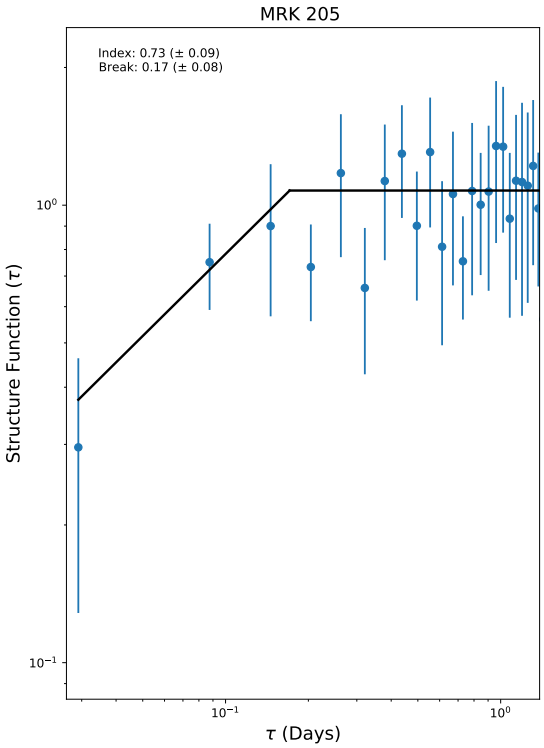
MRK 205
Index: 0.73 (± 0.09)
Break: 0.17 (± 0.08)
Structure Function (τ)
τ (Days)

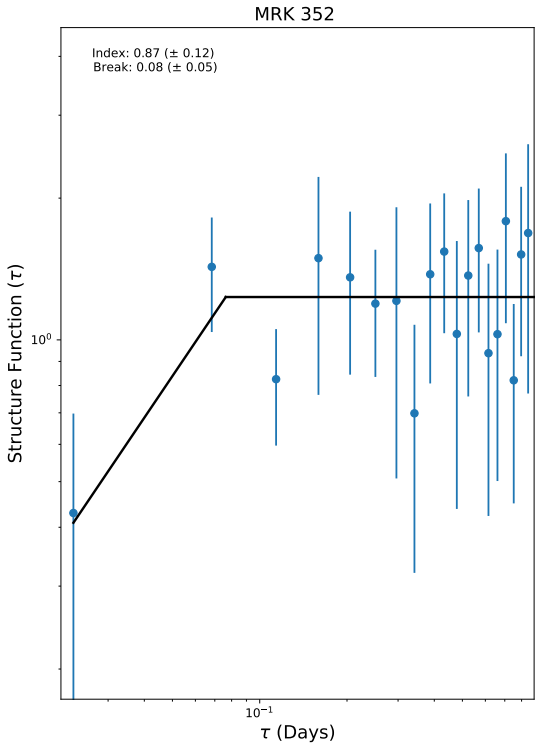
MRK 352
Index: 0.87 (± 0.12)
Break: 0.08 (± 0.05)
Structure Function (τ)
τ (Days)

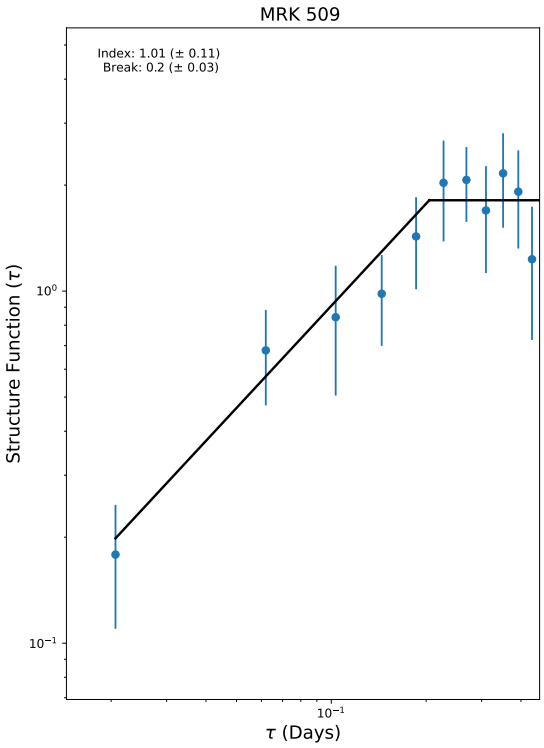
MRK 509
Index: 1.01 (± 0.11)
Break: 0.2 (± 0.03)
Structure Function (τ)
τ (Days)

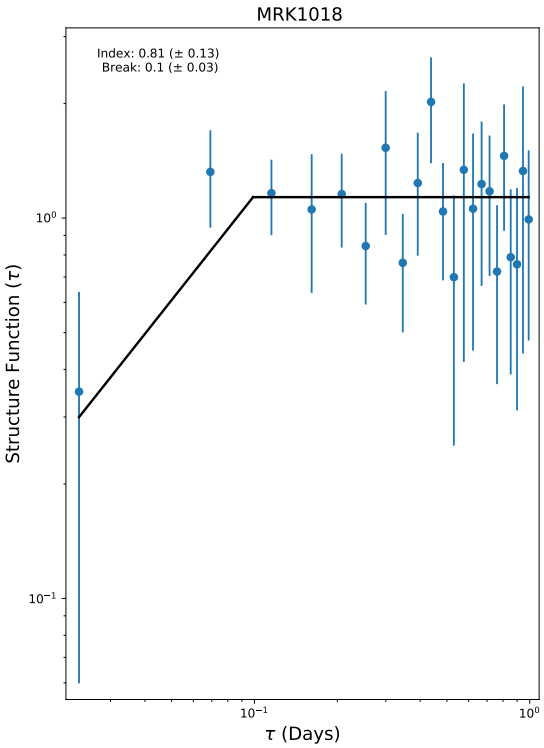
MRK1018
Index: 0.81 (± 0.13)
Break: 0.1 (± 0.03)
Structure Function (τ)
τ (Days)

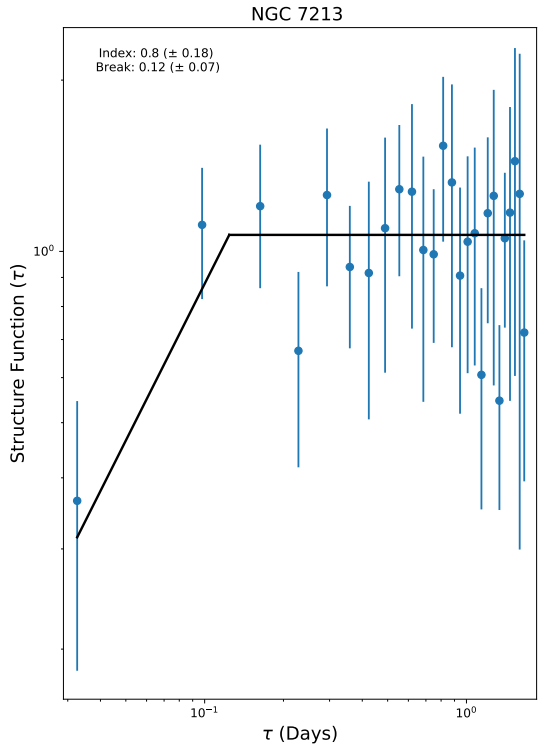
NGC 7213
Index: 0.8 (± 0.18)
Break: 0.12 (± 0.07)
Structure Function (τ)
τ (Days)

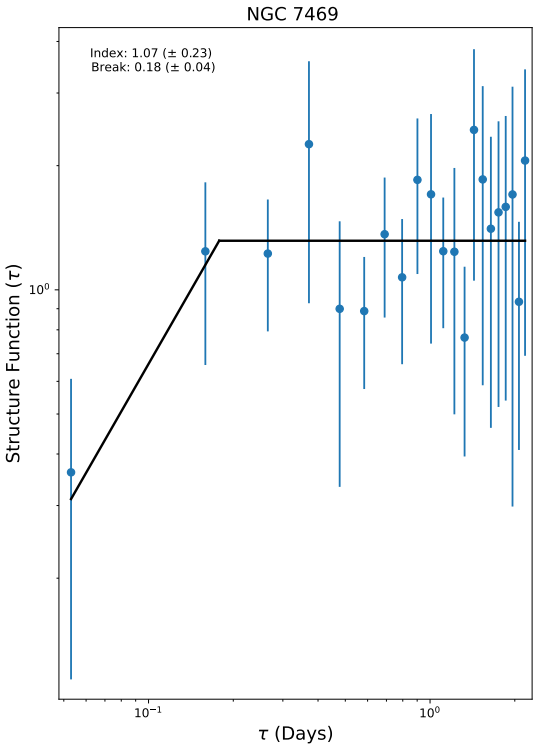
NGC 7469
Index: 1.07 (± 0.23)
Break: 0.18 (± 0.04)
Structure Function (τ)
τ (Days)

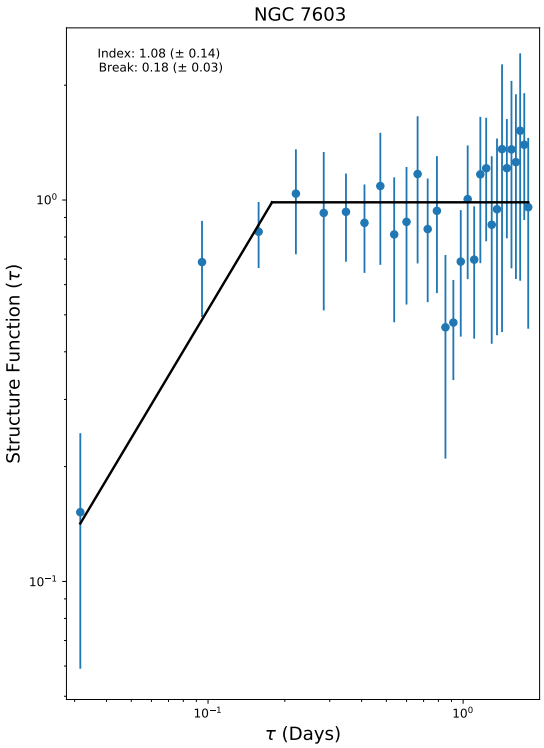
NGC 7603
Index: 1.08 (± 0.14)
Break: 0.18 (± 0.03)
Structure Function (τ)
τ (Days)

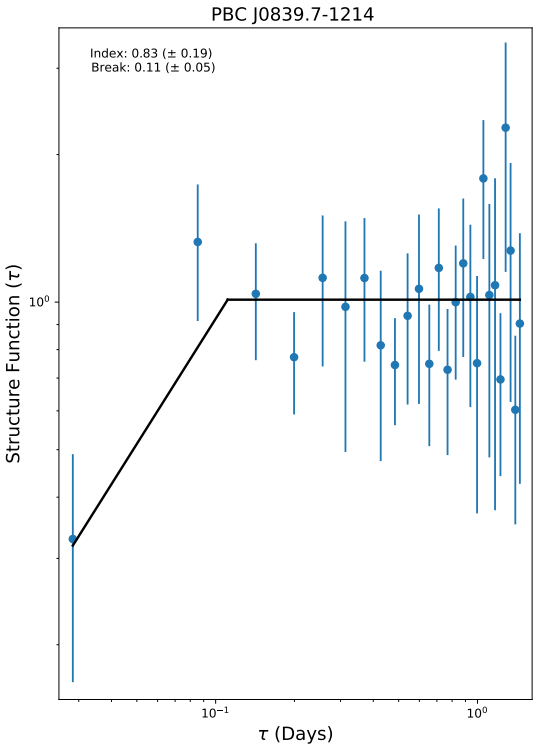
PBC J0839.7-1214
Index: 0.83 (± 0.19)
Break: 0.11 (± 0.05)
Structure Function (τ)
τ (Days)

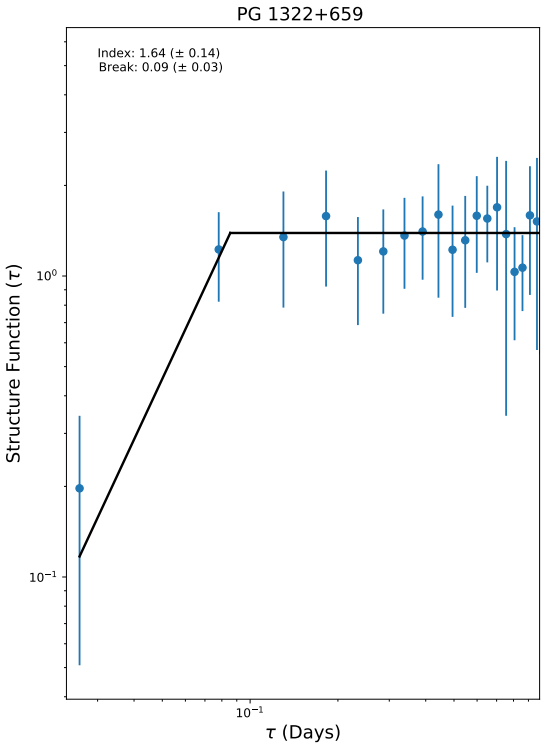
PG 1322+659
Index: 1.64 (± 0.14)
Break: 0.09 (± 0.03)
Structure Function (τ)
τ (Days)

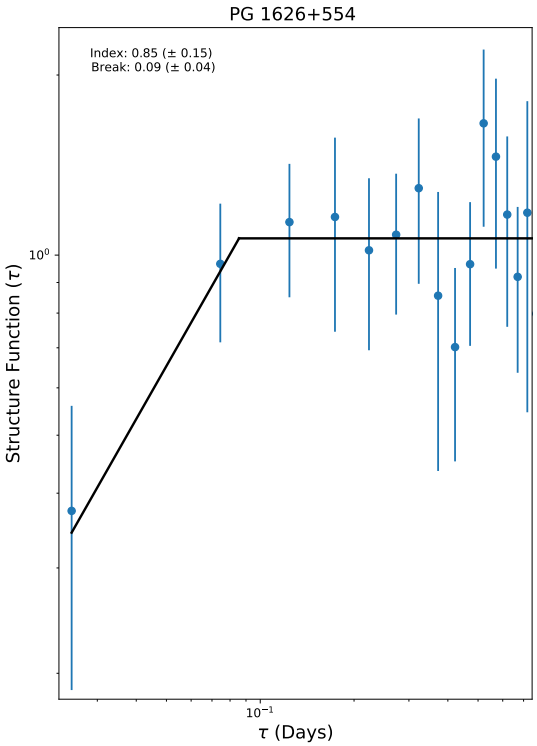
PG 1626+554
Index: 0.85 (± 0.15)
Break: 0.09 (± 0.04)
Structure Function (τ)
τ (Days)

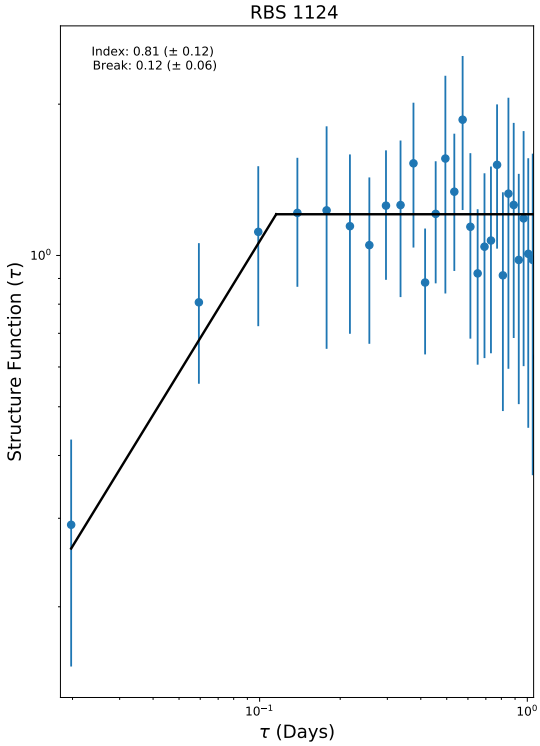
RBS 1124
Index: 0.81 (± 0.12)
Break: 0.12 (± 0.06)
Structure Function (τ)
τ (Days)

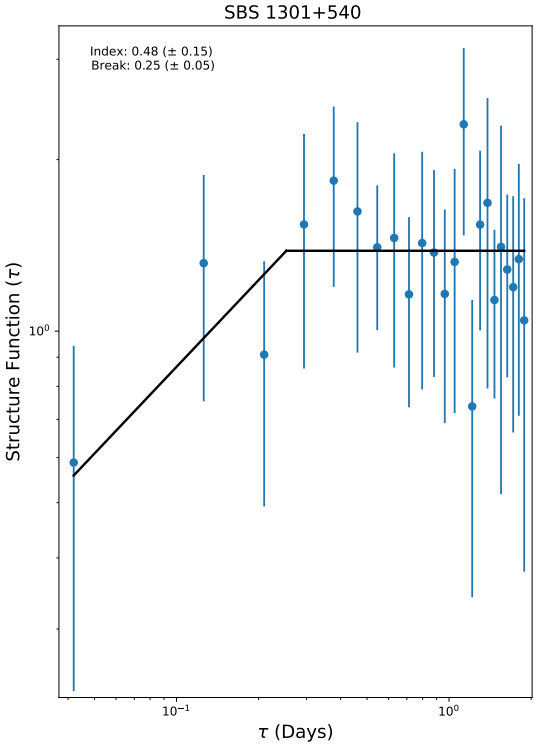
SBS 1301+540
Index: 0.48 (± 0.15)
Break: 0.25 (± 0.05)
Structure Function (τ)
τ (Days)

Bibliography

William N. Alston, Andrew C. Fabian, Erin Kara, Michael L. Parker, Michal Dovciak, and others... A dynamic black hole corona in an active galaxy through X-ray reverberation mapping. *Nature Astronomy*, 4:597–602, January 2020.

P. Barr and R. F. Mushotzky. Limits of X-ray variability in active galactic nuclei. *Nature*, 320:421–423, April 1986.

Th. Boller, T. Liu, P. Weber, R. Arcodia, T. Dauser, J. Wilms, K. Nandra, J. Buchner, A. Merloni, M. J. Freyberg, M. Krumpe, and S. G. H. Waddell. Extreme ultra-soft X-ray variability in an eROSITA observation of the narrow-line Seyfert 1 galaxy 1H 0707-495. A&A, 647:A6, March 2021.

Margaret Z. Buhariwalla, Sophia G. H. Waddell, Luigi C. Gallo, Dirk Grupe, and S. Komossa. Uncovering the Primary X-Ray Emission and Possible Starburst Component in the Polarized NLS1 Mrk 1239. ApJ, 901(2):118, October 2020.

V. R. Chitnis, J. K. Pendharkar, D. Bose, V. K. Agrawal, A. R. Rao, and R. Misra. X-Ray Variability of Active Galactic Nuclei in the Soft and Hard X-Ray Bands. ApJ, 698(2):1207–1220, June 2009.

Stefan Collier and Bradley M. Peterson. Characteristic Ultraviolet/Optical Timescales in Active Galactic Nuclei. ApJ, 555(2):775–785, July 2001.

G. C. Dewangan, K. P. Singh, V. Chavushyan, and J. R. Valdes. The Broad- and Narrow-Line Regions of Narrow-Line Seyfert 1 Galaxies. In J. H. Knapen, J. E. Beckman, I. Shlosman, and T. J. Mahoney, editors, *The Central Kiloparsec of Starbursts and AGN: The La Palma Connection*, volume 249 of *Astronomical Society of the Pacific Conference Series*, page 290, January 2001.

A. C. Fabian, G. Miniutti, L. Gallo, Th. Boller, Y. Tanaka, S. Vaughan, and R. R. Ross. X-ray reflection in the narrow-line Seyfert 1 galaxy 1H 0707-495. MNRAS, 353(4):1071–1077, October 2004.

L. C. Gallo, D. M. Blue, D. Grupe, S. Komossa, and D. R. Wilkins. Eleven years of monitoring the Seyfert 1 Mrk 335 with Swift: Characterizing the X-ray and UV/optical variability. MNRAS, 478(2):2557–2568, August 2018.

L. C. Gallo, W. N. Brandt, E. Costantini, and A. C. Fabian. A longer XMM-Newton look at I Zwicky - 1. Distinct modes of X-ray spectral variability. MNRAS, 377(3): 1375–1382, May 2007.

L. C. Gallo, Y. Tanaka, Th. Boller, A. C. Fabian, S. Vaughan, and W. N. Brandt. Long-term spectral changes in the partial-covering candidate narrow-line Seyfert 1 galaxy 1H 0707-495. MNRAS, 353(4):1064–1070, October 2004.

Luigi C. Gallo. Revealing the Innermost Regions of Active Galaxies. JRASC, 105 (4):143, August 2011.

Marek Gierliński and Chris Done. Is the soft excess in active galactic nuclei real? MNRAS, 349(1):L7–L11, March 2004.

O. González-Martín and S. Vaughan. X-ray variability of 104 active galactic nuclei. XMM-Newton power-spectrum density profiles. A&A, 544:A80, August 2012.

Beth R. Hufnagel and Joel N. Bregman. Optical and Radio Variability in Blazars. ApJ, 386:473, February 1992.

J. S. Kaastra and P. Barr. Soft and hard X-ray variability from the accretion disk of NGC 5548. A&A, 226:59–68, December 1989.

T. Kawaguchi, S. Mineshige, M. Umemura, and Edwin L. Turner. Optical Variability in Active Galactic Nuclei: Starbursts or Disk Instabilities? ApJ, 504(2):671–679, September 1998.

Youjun Lu and Qingjuan Yu. The relationship between X-ray variability and the central black hole mass. *Monthly Notices of the Royal Astronomical Society*, 324(3): 653–658, 06 2001.

A. Markowitz and R. Edelson. An Expanded Rossi X-Ray Timing Explorer Survey of X-Ray Variability in Seyfert 1 Galaxies. ApJ, 617(2):939–965, December 2004.

N. Marshall, R. S. Warwick, and K. A. Pounds. The variability of X-ray emission from active galaxies. MNRAS, 194:987–1002, March 1981.

Ian M. McHardy. X-ray variability of active galactic nuclei. In J. Hunt and B. Battrick, editors, *Two Topics in X-Ray Astronomy, Volume 1: X Ray Binaries. Volume 2: AGN and the X Ray Background*, volume 296 of *ESA Special Publication*, pages 1111–1124, November 1989.

Kazuhisa Mitsuda, Mark Bautz, Hajime Inoue, Richard L. Kelley, Katsuji Koyama, and others... The X-Ray Observatory Suzaku. PASJ, 59:S1–S7, January 2007.

K. Nandra, I. M. George, R. F. Mushotzky, T. J. Turner, and T. Yaqoob. ASCAObservations of seyfert 1 galaxies. i. data analysis, imaging, and timing. ApJ, 476(1): 70–82, feb 1997.

M. Nikolajuk, I. E. Papadakis, and B. Czerny. Black hole mass estimation from X-ray variability measurements in active galactic nuclei. MNRAS, 350(2):L26–L30, May 2004.

M. Nikołajuk, B. Czerny, and P. Gurynowicz. NLS1 galaxies and estimation of their central black hole masses from the X-ray excess variance method. *Monthly Notices of the Royal Astronomical Society*, 394(4):2141–2152, 04 2009.

Hirofumi Noda, Kazuo Makishima, Kazuhiro Nakazawa, Hideki Uchiyama, Shin'ya Yamada, and Soki Sakurai. The Nature of Stable Soft X-Ray Emissions in Several Types of Active Galactic Nuclei Observed by Suzaku. PASJ, 65:4, February 2013.

Paul M. O'Neill, Kirpal Nandra, Iossif E. Papadakis, and T. J. Turner. The relationship between X-ray variability amplitude and black hole mass in active galactic nuclei. MNRAS, 358(4):1405–1416, April 2005.

D. E. Osterbrock and R. W. Pogge. The spectra of narrow-line Seyfert 1 galaxies. ApJ, 297:166–176, October 1985.

I. E. Papadakis. The scaling of the X-ray variability with black hole mass in active galactic nuclei. MNRAS, 348(1):207–213, February 2004a.

Iossif Papadakis. RXTE Variability Study of the Quasars PG 0804+761 and PG 0052+251. RXTE Proposal, January 2004b.

A. R. Patrick, J. N. Reeves, A. P. Lobban, D. Porquet, and A. G. Markowitz. Assessing black hole spin in deep Suzaku observations of Seyfert 1 AGN. MNRAS, 416(4):2725–2747, October 2011.

P. O. Petrucci, D. Gronkiewicz, A. Rozanska, R. Belmont, S. Bianchi, B. Czerny, G. Matt, J. Malzac, R. Middei, A. De Rosa, F. Ursini, and M. Cappi. Radiation spectra of warm and optically thick coronae in AGNs. A&A, 634:A85, February 2020.

C. Pinto, W. Alston, M. L. Parker, A. C. Fabian, L. C. Gallo, D. J. K. Buisson, D. J. Walton, E. Kara, J. Jiang, A. Lohfink, and C. S. Reynolds. Ultrafast outflows disappear in high-radiation fields. MNRAS, 476(1):1021–1035, May 2018.

G. Ponti, I. Papadakis, S. Bianchi, M. Guainazzi, G. Matt, P. Uttley, and N. F. Bonilla. CAIXA: a catalogue of AGN in the XMM-Newton archive. III. Excess variance analysis. A&A, 542:A83, June 2012.

Schmid, H. M., Appenzeller, I., and Burch, U. Spectropolarimetry of the borderline seyfert 1 galaxy eso 323-g077*. *A&A*, 404(2):505–511, 2003.

Małgorzata A. Sobolewska and Chris Done. What is the origin of the soft excess in active galactic nuclei? MNRAS, 374(1):150–158, January 2007.

Tadayuki Takahashi, Keiichi Abe, Manabu Endo, Yasuhiko Endo, Yuuichiro Ezoe, and others... Hard X-Ray Detector (HXD) on Board Suzaku. *Publications of the Astronomical Society of Japan*, 59(sp1):S35–S51, 01 2007.

Yasuo Tanaka, Thomas Boller, Luigi Gallo, Ralph Keil, and Yoshihiro Ueda. Partial Covering Interpretation of the X-Ray Spectrum of the NLS1 1H 0707495. *Publications of the Astronomical Society of Japan*, 56(3):L9–L13, 06 2004.

A. Treves, L. Maraschi, and M. Abramowicz. Basic Elements of the Theory of Accretion. PASP, 100:427, April 1988.

S. Tripathi, K. M. McGrath, L. C. Gallo, D. Grupe, S. Komossa, M. Berton, G. Kriss, and A. L. Longinotti. Tracking the year-to-year variation in the spectral energy distribution of the narrow-line Seyfert 1 galaxy Mrk 335. MNRAS, 499(1):1266–1286, November 2020.

S. Tripathi, S. G. H. Waddell, L. C. Gallo, W. F. Welsh, and C. Y. Chiang. The nature of the soft excess and spectral variability in the Seyfert 1 galaxy Zw 229.015. MNRAS, 488(4):4831–4842, October 2019.

P. Uttley, I. M. McHardy, and I. E. Papadakis. Measuring the broad-band power spectra of active galactic nuclei with RXTE. *Monthly Notices of the Royal Astronomical Society*, 332(1):231–250, 05 2002.

S. Vaughan, R. Edelson, R. S. Warwick, and P. Uttley. On characterizing the variability properties of X-ray light curves from active galaxies. MNRAS, 345(4): 1271–1284, November 2003.

S. G. H. Waddell and L. C. Gallo. A Suzaku sample of unabsorbed narrow-line and broad-line Seyfert 1 galaxies - I. X-ray spectral properties. MNRAS, 498(4): 5207–5226, November 2020.

D. R. Wilkins and L. C. Gallo. Driving extreme variability: the evolving corona and evidence for jet launching in Markarian 335. MNRAS, 449(1):129–146, May 2015.

D. R. Wilkins, E. Kara, A. C. Fabian, and L. C. Gallo. Caught in the act: measuring the changes in the corona that cause the extreme variability of 1H 0707-495. MNRAS, 443(3):2746–2756, September 2014.

Erik Zackrisson. *Quasars and Low Surface Brightness Galaxies as Probes of Dark Matter*. PhD thesis, Department of Astronomy and Space Physics, Uppsala University, Sweden, May 2005.

Xin-Lin Zhou, Shuang-Nan Zhang, Ding-Xiong Wang, and Ling Zhu. Calibrating the Correlation Between Black Hole Mass and X-ray Variability Amplitude: X-ray Only Black Hole Mass Estimates for Active Galactic Nuclei and Ultra-luminous X-ray Sources. ApJ, 710(1):16–23, February 2010.